nature neuroscience

ARTICLES

https://doi.org/10.1038/s41593-020-0684-9

Check for updates

High-fat food biases hypothalamic and mesolimbic expression of consummatory drives

Christopher M. Mazzone[1,9], Jing Liang-Guallpa[2,3,4,9], Chia Li[2,3], Nora S. Wolcott[2], Montana H. Boone[2], Morgan Southern[2], Nicholas P. Kobzar[1], Isabel de Araujo Salgado[2,3], Deepa M. Reddy[2], Fangmiao Sun[5,6,7,8], Yajun Zhang[5,6,7,8], Yulong Li[5,6,7,8], Guohong Cui[1]✉ and Michael J. Krashes[2,3]✉

Maintaining healthy body weight is increasingly difficult in our obesogenic environment. Dieting efforts are often overpowered by the internal drive to consume energy-dense foods. Although the selection of calorically rich substrates over healthier options is identifiable across species, the mechanisms behind this choice remain poorly understood. Using a passive devaluation paradigm, we found that exposure to high-fat diet (HFD) suppresses the intake of nutritionally balanced standard chow diet (SD) irrespective of age, sex, body mass accrual and functional leptin or melanocortin-4 receptor signaling. Longitudinal recordings revealed that this SD devaluation and subsequent shift toward HFD consumption is encoded at the level of hypothalamic agouti-related peptide neurons and mesolimbic dopamine signaling. Prior HFD consumption vastly diminished the capacity of SD to alleviate the negative valence associated with hunger and the rewarding properties of food discovery even after periods of HFD abstinence. These data reveal a neural basis behind the hardships of dieting.

Our brains are tuned to prefer and consume energy-rich foods, such as those high in fats, as an evolutionary mechanism for survival and maturation. However, exposure to these diets can result in overconsumption of calories, leading to obesity and numerous health complications[1,2]. The drive to eat high-fat foods is exacerbated by the subsequent devaluation of less palatable, nutritionally balanced diets. A major gap in knowledge stems from lack of understanding of how this devaluation occurs. Thus, recognizing how brain activity adapts to discrete diets during periods of food exposure and withdrawal, as well as accompanying weight changes, is critical to our ability to develop targeted therapeutics.

Several neural circuits govern the drive to eat for both homeostatic energy needs and the rewarding properties of food[3]. Interoceptive agouti-related peptide (AgRP)-expressing neurons of the hypothalamic arcuate nucleus (ARC) are required for feeding and drive food intake when activated[4–7]. These neurons respond to food presentation, sensory cues of food and direct macronutrient infusion to the gut[8–11]. In line with the unpleasant sensations associated with energy deficit reported in humans, ARC^{AgRP} neurons broadcast a negative valence state in the absence of food[12]. Caloric deprivation and dieting exacerbates this adverse condition, resulting in food seeking to dull this signal. It is suggested that HFD access enhances ARC^{AgRP} activity and might represent a mechanism promoting sustained overconsumption; however, these experiments were carried out in isolated brain slices[13].

Reinforcing dopamine (DA) neurons of the ventral tegmental area (VTA) have been shown to encode the palatability and salience of reward[14–16]. Although ARC^{AgRP} activity can potentiate DA release in response to food, ARC^{AgRP} neurons are not required for consumption of palatable diets[17,18]. Although studies have demonstrated changes in hypothalamic and mesolimbic basal activity after palatable diet exposure[19–25], the endogenous dynamics and function of ARC^{AgRP} neurons and DA signaling in response to a devalued SD remain to be explored. Furthermore, the long-term effects of HFD on these putative activity modifications after HFD withdrawal have yet to be elucidated.

Given that foods with higher fat content are overconsumed and rated as more palatable than lower-calorie foods[26], we hypothesized that HFD exposure would rapidly rewire canonical homeostatic and hedonic nodes in the brain that act to relay incoming caloric information and direct consumption. We employed a multidisciplinary approach to model and study the passive devaluation of a SD in mice after HFD challenge and withdrawal. Our findings reveal that mice forego SD consumption after access to HFD, even in states of caloric deprivation, and that this motivational drive is reflected by altered responses of ARC^{AgRP}, VTA^{DA} neurons and accumbal DA release to food. After HFD exposure, SD is no longer capable of fully suppressing the deleterious affective state of hunger at the level of ARC^{AgRP} neurons or amplifying the appetitive nature of food discovery through mesolimbic DA signaling. These findings reveal how simultaneous preference for HFD and devaluation of SD give rise to overeating and how perturbation of these circuits underlie the familiar complications of dieting.

Results

HFD-induced weight gain and preference. To determine how HFD access affects food intake, body composition and potential HFD-evoked devaluation of SD, we split adult male and female

[1]In Vivo Neurobiology Group, Neurobiology Laboratory, National Institute of Environmental Health Sciences (NIEHS), National Institutes of Health, Research Triangle Park, Durham, NC, USA. [2]Diabetes, Endocrinology, and Obesity Branch, National Institute of Diabetes and Digestive and Kidney Diseases (NIDDK), National Institutes of Health, Bethesda, MD, USA. [3]National Institute on Drug Abuse (NIDA), National Institutes of Health, Baltimore, MD, USA. [4]NIH–Brown University Graduate Program in Neuroscience, Bethesda, MD, USA. [5]State Key Laboratory of Membrane Biology, Peking University School of Life Sciences, Beijing, China. [6]PKU-IDG/McGovern Institute for Brain Research, Beijing, China. [7]Peking-Tsinghua Center for Life Sciences, Academy for Advanced Interdisciplinary Studies, Peking University, Beijing, China. [8]Chinese Institute for Brain Research, Beijing, China. [9]These authors contributed equally: Christopher M. Mazzone, Jing Liang-Guallpa. ✉e-mail: cuig@mail.nih.gov; michael.krashes@nih.gov

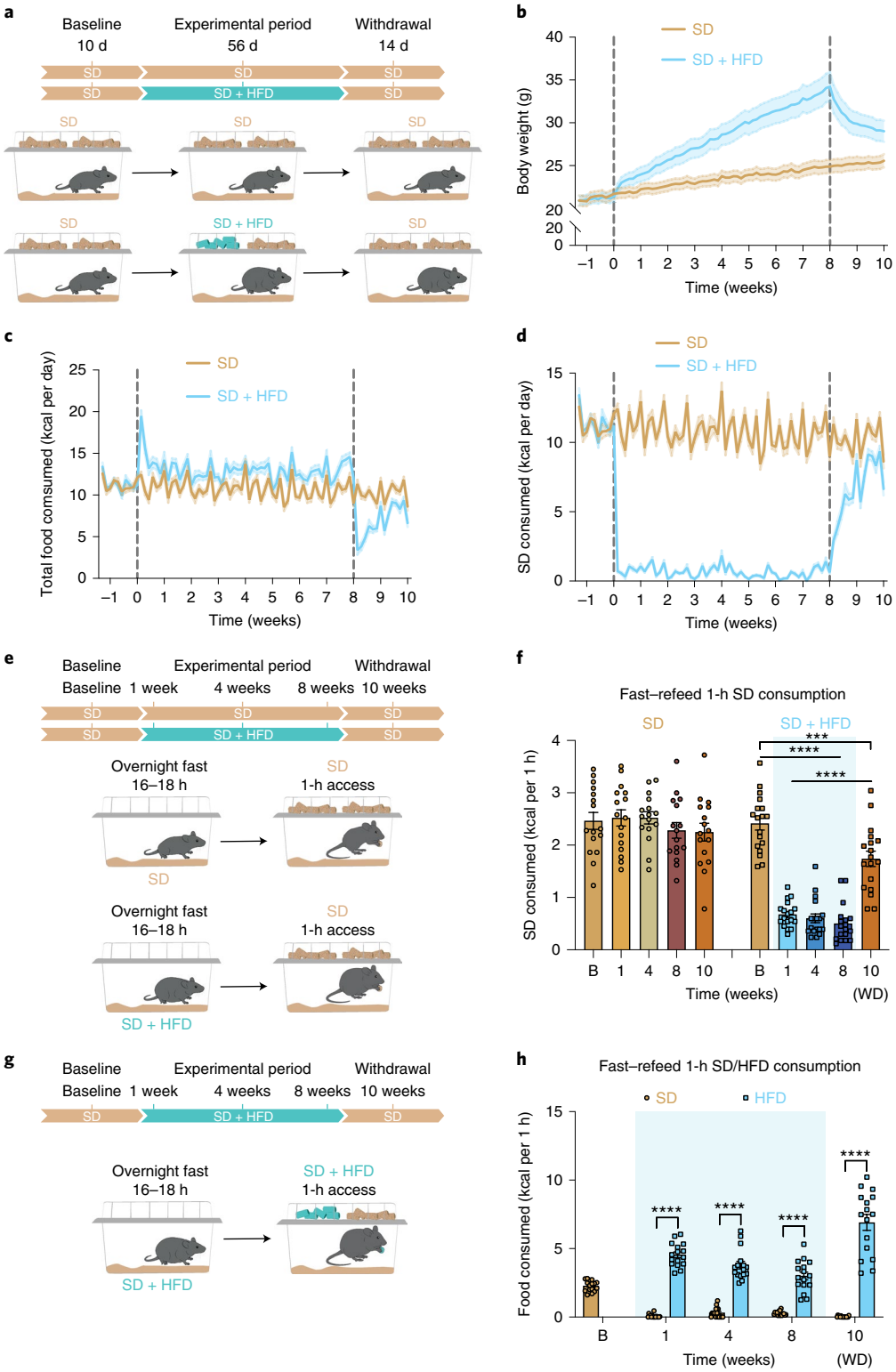

Fig. 1 | HFD exposure promotes weight gain and devaluation of SD. a, Experimental timeline and group schematic for home cage measurements. **b**, Daily body weight ($n=20$ per group, males and females, repeated-measures two-way ANOVA, day × group: $F_{79,3002}=33.34$, $P<0.0001$). **c**, Total food intake ($n=20$ per group, males and females, repeated-measures two-way ANOVA, day × group: $F_{79,3002}=18.73$, $P<0.0001$). **d**, SD intake throughout the duration of the experiment ($n=20$ per group, males and females, repeated-measures two-way ANOVA, day × group: $F_{79,3002}=95.76$, $P<0.0001$). **e**, Experimental timeline and group schematic for fast-refeed test with 1-h SD access. **f**, Within-subject comparison of 1-h SD fast-refeed consumption across testing sessions ($n=16$ SD group, $n=18$ SD + HFD group, males and females, repeated-measures two-way ANOVA, time × group: $F_{4,128}=28.99$, $P<0.0001$, Tukey's multiple comparisons). **g**, Experimental timeline and group schematic for fast-refeed test with 1-h SD and HFD access. **h**, Within-subject comparison of 1-h SD and HFD fast-refeed consumption across testing sessions ($n=16$, males and females, repeated-measures two-way ANOVA, time × diet: $F_{3,90}=30.58$, $P<0.0001$, Tukey's multiple comparisons). Dotted lines in **b**–**d** delineate window of HFD availability. B, baseline; WD, withdrawal. Shaded blue areas in **f** and **h** represent HFD home cage availability. All error bars and shaded regions of **b**–**d** represent mean ± s.e.m. ***$P<0.001$ and ****$P<0.0001$.

wild-type C57BL/6J mice into two groups (Fig. 1a). Both began with ad libitum access to SD (baseline period). One group remained on SD for the duration of the study. The other was supplied ad libitum access to both SD and a 60% HFD for 8 weeks (experimental period), followed by HFD removal for 2 weeks (withdrawal period). Although both groups started with similar weights and daily SD calories consumed, only the HFD-fed mice increased body weight, fat mass and total daily calories consumed without affecting lean mass (Fig. 1b,c and Extended Data Fig. 1a–c; for full statistical results, see Supplementary Table 1). HFD-exposed mice exhibited an immediate preference for the HFD in lieu of SD (Fig. 1d and Extended Data Fig. 1d). As previously reported, genetically identical mice exhibited a wide range of body weight changes due to HFD exposure (Extended Data Fig. 1c)[27]. Notably, every mouse exposed to HFD showed a marked reduction of SD intake, and there was no correlation between the average amount of SD consumed during the experimental period and total body weight change after the experimental period (Extended Data Fig. 1d,e). Removal of HFD resulted in precipitous weight loss due to the failure of mice to consume the required daily calories from SD[28], thus emphasizing a potential HFD-induced devaluation of SD to the point of self-restricted caloric deprivation (Fig. 1b–d). Body weight, fat mass levels and daily calories consumed did not recover to SD control values even after 2 weeks of HFD withdrawal, indicating prolonged physiological adaptations after HFD challenge (Fig. 1b–d and Extended Data Fig. 1a)[28].

Devaluation of SD during periods of hunger. To assess whether HFD exposure changes the valuation and subsequent consumption of SD during periods of physiological hunger, we food deprived a separate cohort of mixed-sex, adult mice overnight and then measured SD consumption over a 1-h refeeding session (Fig. 1e). We longitudinally tested fast–refeed SD consumption in mice before access to HFD (baseline) at 1, 4 and 8 weeks during home cage HFD access and after 2 weeks of HFD withdrawal (Fig. 1e). As a control, mice maintained on ad libitum SD were tested in parallel. Mice maintained strictly on SD showed consistent SD caloric intake across the experimental time course, whereas HFD-exposed mice exhibited a stark reduction in SD intake during the refeeding sessions compared both to their response at baseline (Fig. 1f) and to the SD group at each time point (Extended Data Fig. 1f). This passive devaluation remained intact, although to a lesser degree, during the withdrawal period (Fig. 1f and Extended Data Fig. 1f). Critically, the SD devaluation across sessions did not correlate with changes in body weight across the experiment (Extended Data Fig. 1g). To further uncouple changes in body weight from SD devaluation after HFD exposure, a new cohort of animals, including a group of HFD-fed animals yoked to match the weights of the ad libitum SD group, displayed a similar devaluation of SD after a fast–refeed, although this returned to baseline levels 2 weeks after HFD withdrawal (Extended Data Fig. 1h–j). To ensure that HFD-challenged animals were still motivated to eat, we repeated the fast–refeed test sessions with access to both SD and HFD after fasting (Fig. 1g). During the experimental period, mice exposed to HFD robustly consumed HFD to greater caloric values than baseline consumption of SD while minimally consuming SD (Fig. 1h and Extended Data Fig. 1k). Interestingly, the amount of HFD calories consumed during the 1-h refeeding period diminished the longer animals were exposed to HFD (Extended Data Fig. 1k). In agreement with intermittent binge models, consumption of HFD during a fast–refeed session was further pronounced after HFD withdrawal (Fig. 1h and Extended Data Fig. 1k)[29].

Our data demonstrate that lean animals exposed to HFD showed devaluation toward SD, and this occurred independent of weight gain (Extended Data Fig. 1g–j). To test this model in hyperphagic, genetically obese animals and to determine the functional contribution of two classic satiety signaling pathways, we repeated the experimental design using two mouse models of obesity: those lacking the melanocortin-4 receptor (MC4R KO) and those incapable of producing leptin (leptin KO; Extended Data Fig. 2a,d)[30,31]. Despite being obese from the start of the experiment, HFD-fed MC4R KO and leptin KO mice exhibited similar devaluation of SD during a fast–refeed period compared to their heterozygous littermate controls (Extended Data Fig. 2a–f).

In the experiments above, the earliest time point tested was 1 week after HFD access when body weights on average began deviating and metabolic changes have been reported[32]. To determine whether HFD alters fasting-induced feeding of SD before metabolic changes, we repeated the experiment in mice subjected to HFD for only 24 h (Extended Data Fig. 2g). After overnight food deprivation, mice that were provided HFD for 24 h showed reduced SD intake than baseline measurements and littermate, HFD-naive control mice (Extended Data Fig. 2h–i). Collectively, these results demonstrate that HFD exposure rapidly, profoundly and lastingly reduced SD intake in varying physiological conditions, independent of sex, diet-induced body weight changes, functional MC4R or leptin signaling or preexisting obesity.

Modified hypothalamic responses to SD after HFD exposure. The sensory detection and subsequent consumption of food rapidly suppresses ARC^{AgRP} activity, serving to silence the negative valence associated with hunger[8,9,12]. To determine how HFD exposure

Fig. 2 | HFD-exposure alters ARC^{AgRP} activity responses to SD and HFD in fasted mice. a, Left: brain schematic of unilateral viral delivery of Cre-inducible GCaMP6s to the ARC of AgRP-ires-Cre; Ai9-tdTomato reporter mice and optical fiber implant. Right: representative image of GCaMP6s and tdTomato expression. **b**, Experimental timeline and group schematic for fasted photometry recordings. **c**–**d**, Average fasted photometry traces of the (**c**) SD group and (**d**) SD + HFD group across recording sessions aligned to Pellet 1 and 2 presentation ($n = 12$ SD group, $n = 11$ SD + HFD group, males and females). **e**, Within-subject quantification of fasted ARC^{AgRP} activity response to Pellet 1 (SD) ($n = 12$ SD group, $n = 11$ SD + HFD group, males and females, repeated-measures two-way ANOVA, time × group: $F_{5, 105} = 16.74$, $P < 0.0001$, Bonferroni's multiple comparisons). **f**, SD consumed across testing sessions during the first 5 min of food access ($n = 12$ SD group, $n = 11$ SD + HFD group, males and females, repeated-measures two-way ANOVA, time × group: $F_{5, 105} = 15.81$, $P < 0.0001$, Bonferroni's multiple comparisons). **g**, Within-subject quantification of fasted ARC^{AgRP} activity response to Pellet 2 (SD for SD group; SD for SD + HFD group during B1 and B2 and HFD for SD + HFD group during 1, 4, 8 and 10 weeks) ($n = 12$ SD group, $n = 11$ SD + HFD group, males and females, repeated-measures two-way ANOVA, time × group: $F_{5, 105} = 21.07$, $P < 0.0001$, Bonferroni's multiple comparisons). **h**, Total calories consumed across testing sessions ($n = 12$ SD group, $n = 11$ SD + HFD group, males and females, repeated-measures two-way ANOVA, time × group: $F_{5, 105} = 14.26$, $P < 0.0001$, Bonferroni's multiple comparisons). **i**,**j**, Average fasted photometry traces of the (**i**) SD group and (**j**) SD + HFD group across recording sessions aligned to Pellet 1 (SD) consumption. **k**, Within-subject quantification of fasted ARC^{AgRP} activity response to Pellet 1 (SD) consumption ($n = 12$ SD group, $n = 8$–11 SD + HFD group, males and females, mixed-effects model, time × group: $F_{5,99} = 3.735$, $P = 0.0039$, Bonferroni's multiple comparisons). Dotted lines in **c** and **d** indicate Pellet 1 and Pellet 2 presentation. Dotted lines in **i** and **j** indicate Pellet 1 consumption. Shaded blue areas in **e**–**h** and **k** represent HFD home cage availability. B1 and B2 refer to Baseline 1 and 2, respectively. WD, withdrawal. All error bars and shaded regions of **c**, **d**, **i** and **j** represent s.e.m. $^{*}P < 0.05$, $^{**}P < 0.01$, $^{***}P < 0.001$ and $^{****}P < 0.0001$.

affects ARC^{AgRP} responses to food, we longitudinally recorded ARC^{AgRP} population activity using the fluorescent calcium sensor GCaMP6s[33] as both male and female mice transitioned to and from HFD (Fig. 2a,b). GCaMP6s-expressing mice were maintained on SD and underwent two baseline recordings in both the fed and fasted conditions before half of the mice were supplied HFD using the timeline described (Fig. 2b). At baseline, all mice were provided an SD pellet (Pellet 1) to their home cage while recording ARC^{AgRP} activity. Five minutes later, a second SD pellet (Pellet 2) was added for an additional 5 min (Fig. 2b). Once the HFD group was exposed to HFD, the second pellet (Pellet 2) during recording sessions was a HFD pellet for this group only (Fig. 2b).

During both baseline recordings, we observed robust inhibition of ARC^{AgRP} neurons by SD Pellet 1 presentation in all fasted animals; this was accompanied by similar SD intake in each session (Fig. 2c–f and Extended Data Fig. 3a,b). Whereas this response to SD Pellet 1 was consistent across time in mice maintained on SD, those provided with HFD had significantly reduced population responses to

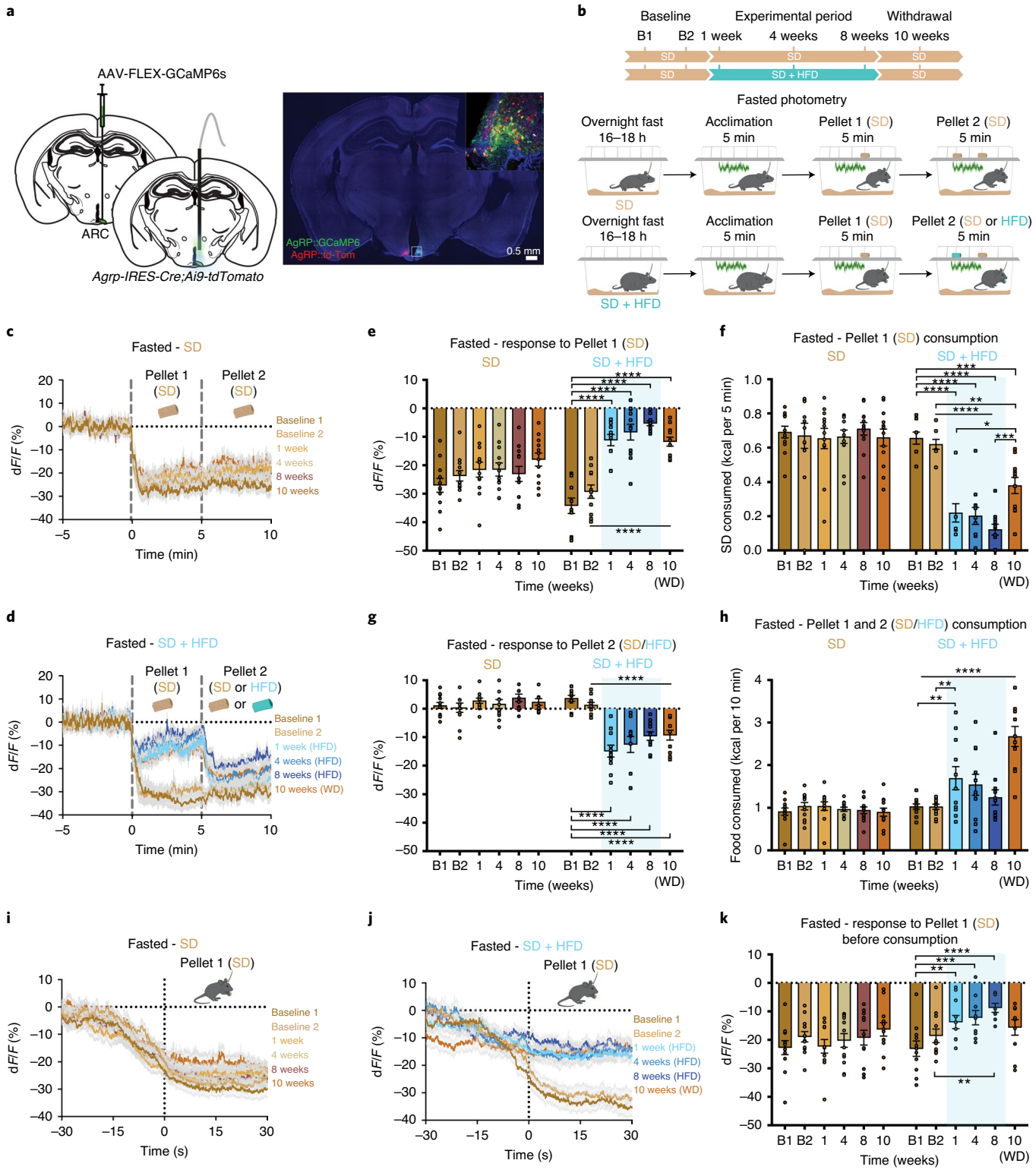

SD Pellet 1 compared to both their baseline response and control mice maintained on SD (Fig. 2c–f and Extended Data Fig. 3a,b). Although this attenuated ARC^{AgRP} response to SD Pellet 1 corresponded with a reduction in the amount of SD consumed during the 5-min window (Fig. 2e,f and Extended Data Fig. 3a,b), ARC^{AgRP} inhibition was blunted before food intake in the HFD-exposed animals (Fig. 2j,k). Notably, this sensory-evoked ARC^{AgRP} inhibition to SD preceding consumption remained constant in HFD-naive animals (Fig. 2i,k). Remarkably, diminished ARC^{AgRP} inhibition to SD Pellet 1 was still present after a 2-week withdrawal from HFD, akin to a strict diet, emphasizing the enduring effect that HFD exposure has on this signaling system (Fig. 2d–f and Extended Data Fig. 3a,b). Furthermore, the change in ARC^{AgRP} dynamics in response to SD Pellet 1 were largely independent of body weight change throughout the experiment (Extended Data Fig. 3c–f). In summary, although SD Pellet 1 presentation stably reduced ARC^{AgRP} activity in HFD-naive mice, it was no longer capable of silencing the negative affective state linked to hunger (encoded by ARC^{AgRP} neurons) after HFD challenge. These results provide a potential neural mechanism for why SDs lose their capacity to curb hunger after prior access to palatable foods.

The addition of a second SD Pellet 2 did not further inhibit ARC^{AgRP} activity in SD mice (Fig. 2c,g); however, presentation of an HFD Pellet 2 promoted additional inhibition of ARC^{AgRP} neurons in HFD-exposed mice (Fig. 2d,g and Extended Data Fig. 3g). Therefore, the diminished response to SD Pellet 1 in HFD-challenged mice was not due to a floor effect or impairment of ARC^{AgRP} activity but to a preference for HFD as evidenced by total food consumption during this window (Fig. 2h and Extended Data Fig. 3h).

To determine how rapidly this devaluation of SD and proclivity for HFD consumption occurs in ARC^{AgRP} neurons, we repeated this experiment with mice that were provided access to HFD for only 24 h (Extended Data Fig. 3i). At baseline, before HFD exposure, all mice displayed a robust inhibition of ARC^{AgRP} activity in response to SD Pellet 1, and this effect remained constant after the addition of SD Pellet 2 (Extended Data Fig. 3j–n). However, just 24 h of home cage HFD exposure led to a significant reduction of ARC^{AgRP} inhibition and intake of SD Pellet 1 (Extended Data Fig. 3j–l). HFD Pellet 2 presentation reversed this blunted ARC^{AgRP} inhibition in all HFD-exposed mice, corresponding to increased calories consumed (Extended Data Fig. 3j, m–n). Thus, we observed a similar short- and long-term devaluation of SD in HFD-challenged mice.

There were minimal changes in ARC^{AgRP} activity upon introduction of SD Pellet 1 across all conditions and time points under fed (sated) conditions, corresponding to nominal chow consumption (Extended Data Fig. 4a–g). Although the addition of SD Pellet 2 failed to alter ARC^{AgRP} activity over time in HFD-naive mice, presentation of HFD Pellet 2 to the HFD-exposed group significantly suppressed ARC^{AgRP} activity 1 week into HFD challenge when the diet was still relatively new (Extended Data Fig. 4b–c, h–i). This response dissipated at 4 and 8 weeks, only to reemerge after a 2-week HFD withdrawal (Extended Data Fig. 4c, h–i). Thus, consumption of HFD under satiation acted to further suppress the negative valence signal associated with these cells[12], an effect potentiated after HFD restriction. Collectively, these observations provide a plausible neural process behind the tendency to consume energy-dense foods in the calorically replete state.

A previous study indicated that HFD-induced obesity altered the intrinsic properties of ARC^{AgRP} neurons by increasing firing rate and resting membrane potential[13]. Although we observed a similar phenomenon in isolated brain slices (data not shown), these between-group studies were performed devoid of neural input. Here, using spectrum-based, longitudinal fiber photometry recordings, we were able to capture the putative changes of ARC^{AgRP} basal activity after HFD exposure (Extended Data Fig. 5a). HFD access reduced resting ARC^{AgRP} activity relative to the SD group in both the fed and fasted states (Extended Data Fig. 5b). Despite this robust decline in basal activity, fasting increased observed GCaMP fluorescence by ~50% relative to the sated state, suggesting similar magnitudes of fasting-induced enhancements of ARC^{AgRP} activity regardless of HFD history (Extended Data Fig. 5c). Counter to ex vivo slice experiments, these findings demonstrate that HFD challenge, similar to the acute effects of alcohol and non-nutritive drugs[17], negatively shifted basal ARC^{AgRP} activity during HFD exposure.

ARC^{AgRP} neurons receive dense GABAergic input from leptin receptor (LepR)-expressing neurons in the dorsomedial hypothalamus (DMH) that have opposing responses to food[34]. To ascertain whether similar HFD-induced alterations occurred in this upstream circuit, we took a two-pronged approach and measured the effect of HFD challenge on both the synaptic plasticity of this DMH^{LepR}→ARC^{AgRP} connection and the in vivo DMH^{LepR} population dynamics in response to food. Channelrhodopsin-2 (ChR2) was targeted to DMH^{LepR} neurons, and light-evoked, paired-pulse experiments were performed in ARC$^{Npy/AgRP}$ neurons (Fig. 3a,b). Notably, 98% of AgRP neurons co-express NPY[35]. Chronic HFD significantly increased the paired-pulse ratio of light-evoked, post-synaptic inhibitory currents from DMH^{LepR} neurons onto ARC^{AgRP} neurons, reflecting a reduced probability of GABAergic release from these synapses (Fig. 3b). Although this input likely does not reflect the source of HFD-induced decreases in basal ARC^{AgRP} activity revealed in our photometry recordings, it nonetheless emphasizes larger-scale intrahypothalamic circuit dynamics influenced by HFD.

To assess how this intrahypothalamic input might contribute to altered ARC^{AgRP} responses to food, we selectively expressed

Fig. 3 | HFD exposure induces alterations in DMH^{LepR} responses to SD. a, Left: brain schematic of unilateral viral delivery of Cre-inducible ChR2 to the DMH of LepR-ires-Cre;Npy-hrGFP mice and position of ex vivo slice recordings from ARC^{Npy} cells. Right: representative image of ARC slice showing NPY-hrGFP and DMH^{LepR}::ChR2 terminals. **b**, Top: schematic of light-evoked, paired-pulse recordings. Left: representative traces. Right: quantification of ratio ($n = 37$ cells per four mice in the SD group and 31 cells per four mice in the SD + HFD group, unpaired t-test (two tailed) with Welch's correction, $P = 0.0152$). **c**, Left: brain schematic of unilateral viral delivery of Cre-inducible GCaMP6s to the DMH of LepR-ires-Cre mice and optical fiber implant. Right: representative image of GCaMP6s expression. **d**, Experimental timeline and group schematic for both fasted and fed photometry recordings. **e**, Average fasted photometry traces across recording sessions aligned to Pellet 1 and 2 presentation ($n = 9$, males and females). **f**, Within-subject quantification of fasted DMH^{LepR} activity response to Pellet 1 (SD) and Pellet 2 (SD at baseline; HFD during 1, 4 and 5 weeks) ($n = 9$, males and females, repeated-measures two-way ANOVA, time × pellet: $F_{3,48} = 11.07$, $P < 0.0001$, Tukey's multiple comparisons). **g**, Total calories consumed across testing sessions ($n = 9$, males and females, repeated-measures two-way ANOVA, time × pellet: $F_{3,48} = 66.65$, $P < 0.0001$, Tukey's multiple comparisons). **h**, Average fed photometry traces across recording sessions aligned to Pellet 1 and 2 presentation ($n = 9$, males and females). **i**, Within-subject quantification of fed DMH^{LepR} activity response to Pellet 1 (SD) and Pellet 2 (SD at baseline; HFD during 1, 4 and 5 weeks) ($n = 9$, males and females, repeated-measures two-way ANOVA, time × pellet: $F_{3,48} = 14.44$, $P < 0.0001$, Tukey's multiple comparisons). **j**, Total calories consumed across testing sessions ($n = 9$, males and females, repeated-measures two-way ANOVA, time × pellet: $F_{3,48} = 81.11$, $P < 0.0001$, Tukey's multiple comparisons). Dotted lines in **e** and **h** indicate Pellet 1 and Pellet 2 presentation. Shaded blue areas in **f**, **g**, **i** and **j** represent HFD home cage availability. B, baseline; WD, withdrawal. All error bars and shaded regions of **e**–**h** represent s.e.m. *$P < 0.05$, **$P < 0.01$, ***$P < 0.001$ and ****$P < 0.0001$.

GCaMP6s in DMH^{LepR} neurons, thus providing longitudinal access to activity dynamics to food presentation before, during and after HFD challenge in both the fasted and fed conditions (Fig. 3c,d). We found that HFD exposure significantly dampened the baseline DMH^{LepR} population response to and consumption of SD Pellet 1 in hungry mice, an effect still present after HFD withdrawal (Fig. 3e–g). Although presentation of SD Pellet 2 in hungry HFD-naive mice increased activity, this was strongly amplified by the introduction of HFD Pellet 2 after home cage HFD exposure, resulting in higher caloric intake (Fig. 3e–g). Food intake and activity changes to SD Pellet 1 were minimal in the fed condition (Fig. 3h–j). However, we found that addition of HFD Pellet 2 in fed mice significantly altered DMH^{LepR} activity 1 week after HFD exposure, and this effect was further heightened after HFD withdrawal when intake was high (Fig. 3h–j). A reduction in GABAergic transmission from DMH^{LepR}→ARC^{AgRP} neurons would agree with the diminished

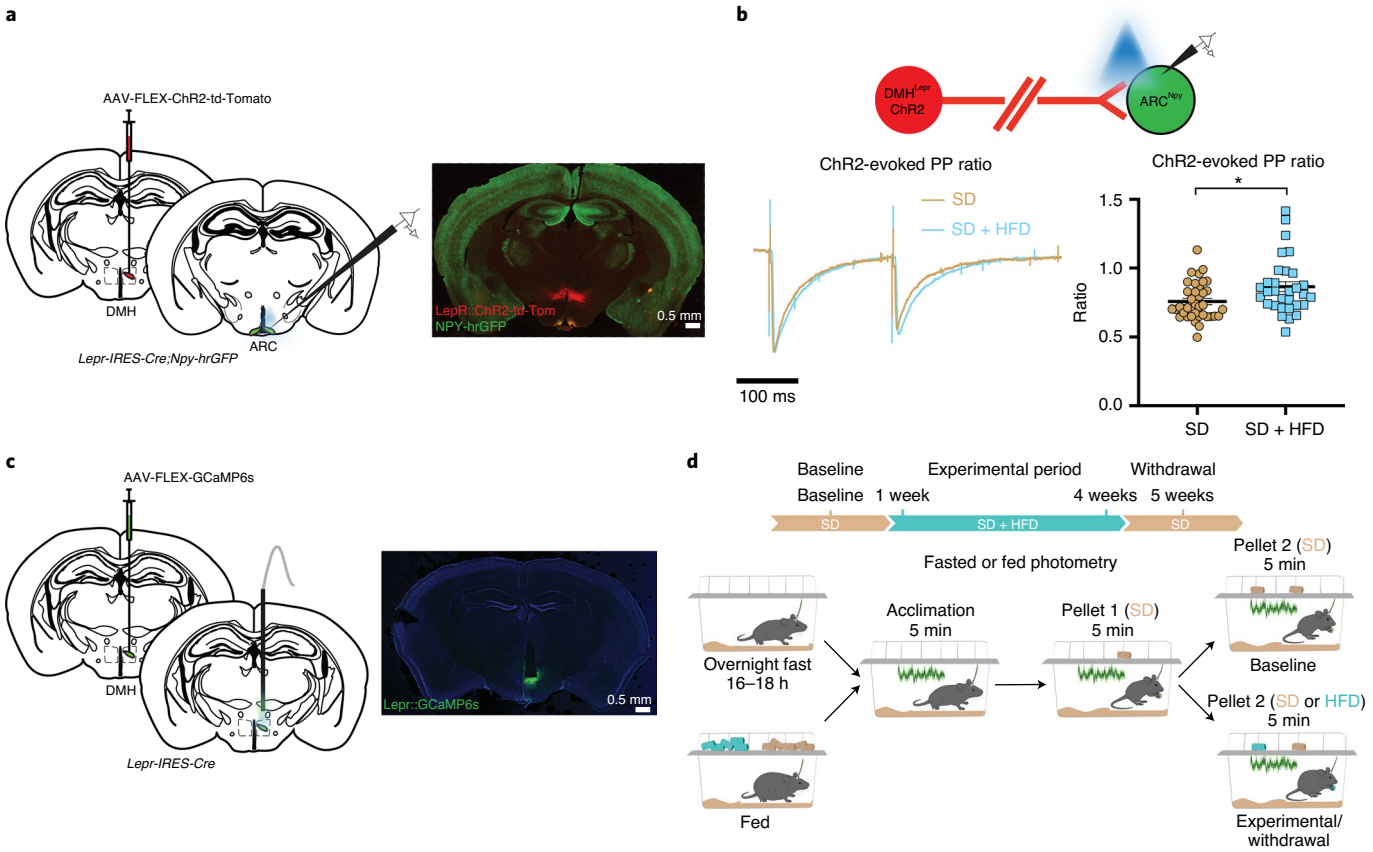

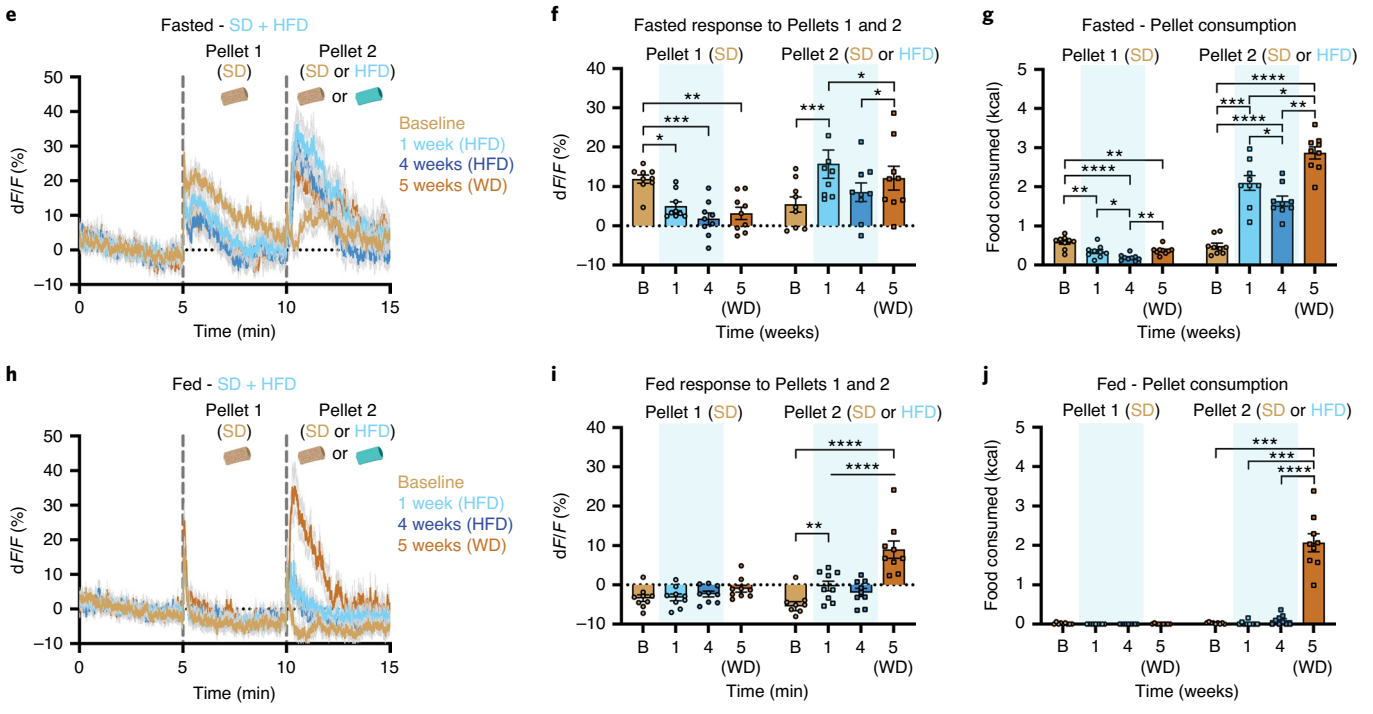

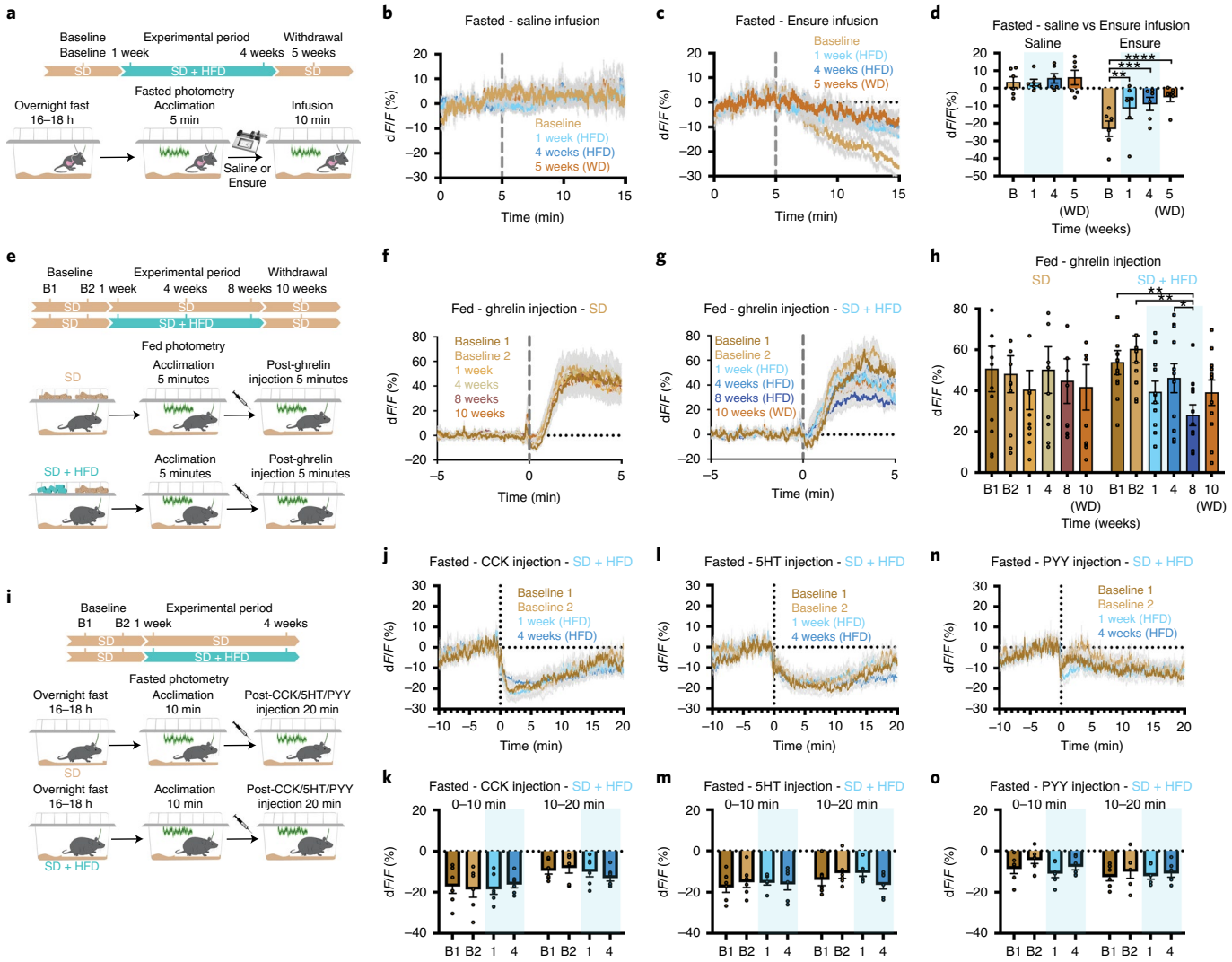

Fig. 4 | HFD-exposure disrupts ARC^{AgRP} responses to both peripheral detection of calories and signals of hunger. a, Experimental timeline and group schematic for fasted photometry recordings during gastric infusions. **b**,**c**, Average fasted ARC^{AgRP} photometry traces in response to gastric infusion of (**b**) saline or (**c**) Ensure ($n = 6$, males and females). **d**, Within-subject quantification of fasted ARC^{AgRP} activity response to gastric infusions of saline or Ensure across testing sessions ($n = 6$, males and females, repeated-measures two-way ANOVA, time × infusion: $F_{3,15} = 7.236$, $P = 0.0032$, Tukey's multiple comparisons). **e**, Experimental timeline and group schematic for fed photometry recordings during ghrelin injection. **f**,**g**, Average photometry traces of the (**f**) SD group and (**g**) SD + HFD group across recording sessions aligned to ghrelin injection ($n = 12$ SD group, $n = 11$ SD + HFD group, males and females). **h**, Within-subject quantification of ARC^{AgRP} activity to ghrelin across testing sessions ($n = 12$ SD group, $n = 11$ SD + HFD group, males and females, repeated-measures two-way ANOVA, time × group: $F_{5,105} = 3.244$, $P = 0.0092$, Tukey's multiple comparisons). **i**, Experimental timeline and group schematic for fasted photometry recordings during CCK, 5-HT or PYY injection. **j**,**l**,**n**, Average photometry traces of the SD + HFD group across recording sessions aligned to (**j**) CCK, (**l**) 5-HT or (**n**) PYY injection ($n = 6$ SD + HFD group, males and females). **k**,**m**,**o**, Within-subject quantification of ARC^{AgRP} activity to (**k**) CCK ($n = 6$ SD + HFD group, males and females, repeated-measures two-way ANOVA, time bin × week: $F_{1.681,8.404} = 3.230$, $P = 0.0961$), **m**, 5-HT ($n = 6$ SD + HFD group, males and females, repeated-measures two-way ANOVA, time bin × week: $F_{1.656,8.279} = 2.904$, $P = 0.1158$) or (**o**) PYY ($n = 6$ SD + HFD group, males and females, repeated-measures two-way ANOVA, time bin × week: $F_{2.081,10.40} = 2.203$, $P = 0.1583$) across testing sessions. Dotted lines indicate (**b**, **c**) infusion, (**f**, **g**) ghrelin, (**j**) CCK, (**l**) 5-HT or (**n**) PYY injection. Shaded blue areas in **d**, **h**, **k**, **m** and **o** represent HFD home cage availability. B1 and B2 refer to Baseline 1 and 2, respectively. WD, withdrawal. All error bars and shaded regions of **b**, **c**, **f**, **g**, **j**, **l** and **n** represent s.e.m. $^*P < 0.05$, $^{**}P < 0.01$, $^{***}P < 0.001$ and $^{****}P < 0.0001$.

inhibition to SD that we observed in ARC^{AgRP} neurons after HFD access (Fig. 2). Together, this highlights the long-term effect of HFD on multiple hypothalamic nuclei and motivated feeding.

To establish whether exposure to HFD perturbs ARC^{AgRP} activity independent of sensory food detection, we longitudinally recorded population dynamics in mice either infused with calories directly into the stomach or injected with a panel of peptides and hormones before, during and after HFD challenge (Fig. 4). Infusion of non-caloric saline had no effect on ARC^{AgRP} activity over time (Fig. 4a,b,d). Gastric infusion of calories (0.86 kcal of Ensure) durably reduced ARC^{AgRP} dynamics[10,11], but we found that home cage HFD exposure severely blunted ARC^{AgRP} activity to the same caloric load during and after HFD challenge (Fig. 4c,d). This change in activity was tightly correlated to body weight after 1 week of HFD exposure but grew weaker over time (Extended Data Fig. 6a).

Given this rapid change in gut–brain communication, we reasoned that the effects of stomach-secreted peptides and hormones might no longer be as potent in modulating ARC^{AgRP} activity after

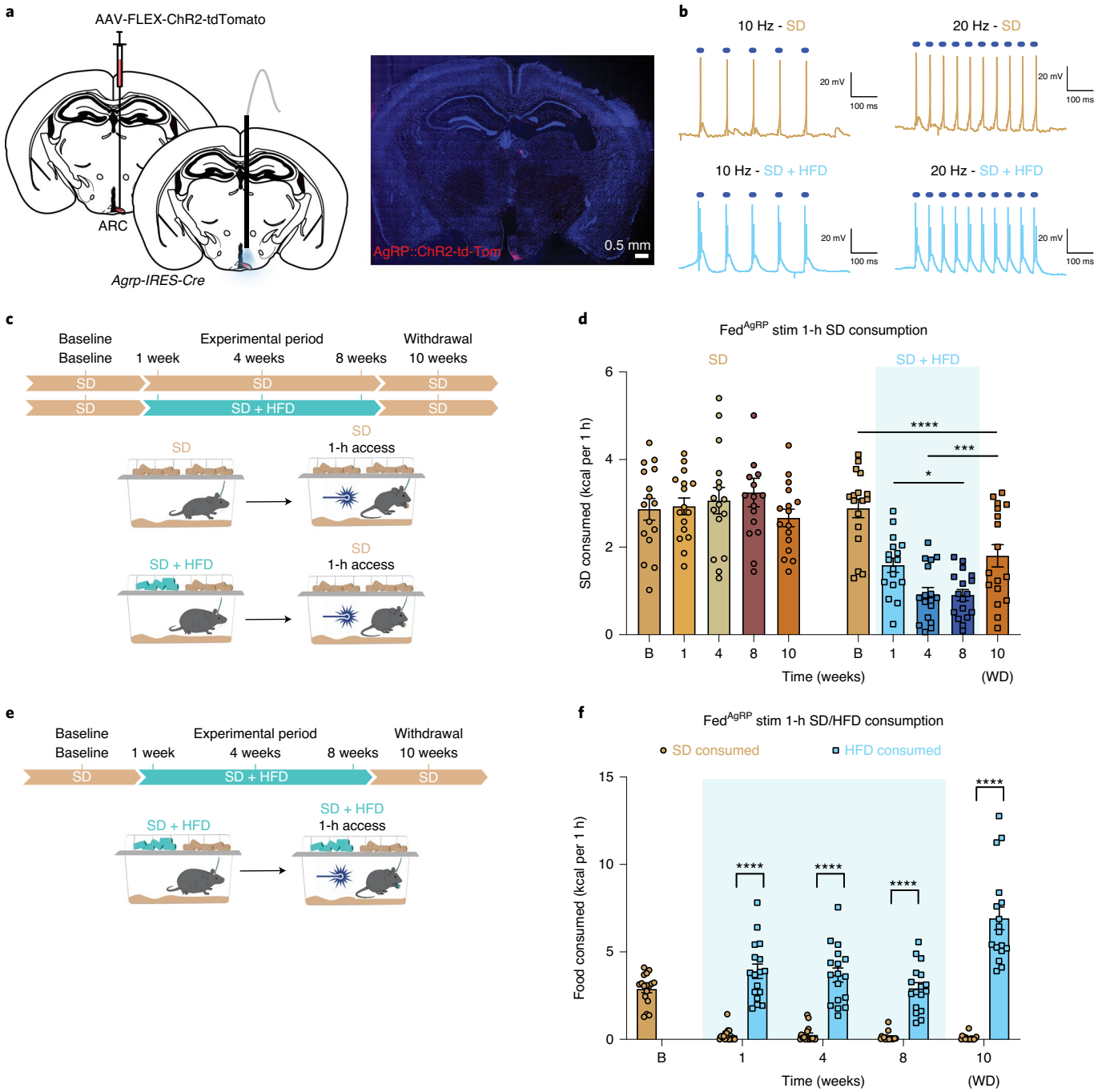

Fig. 5 | HFD-exposure disrupts functional capacity of ARC^{AgRP} neurons to drive SD, but not HFD, consumption. a, Left: brain schematic of unilateral viral delivery of Cre-inducible ChR2-tdTomato to the ARC of AgRP-ires-Cre mice and optical fiber implant. Right: representative image of ChR2-tdTomato expression. **b**, Light-evoked action potentials in AgRP::ChR2 mice in SD (top) and SD + HFD (bottom) groups. **c**, Experimental timeline and group schematic for optogenetic studies with 1-h SD access. **d**, Within-subject comparison of Fed^{AgRP} stimulation 1-h SD consumption across testing sessions ($n = 16$ SD group, $n = 17$ SD + HFD group, males and females, repeated-measures two-way ANOVA, time × group: $F_{4, 124} = 18.85$, $P < 0.0001$, Tukey's multiple comparisons). **e**, Experimental timeline and group schematic for optogenetic studies with 1-h SD and HFD access. **f**, Within-subject comparison of Fed^{AgRP} stimulation 1-h SD and HFD consumption across testing sessions ($n = 17$, males and females, repeated-measures two-way ANOVA, time × diet: $F_{3,96} = 26.03$, $P < 0.0001$, Bonferroni's multiple comparisons). Shaded blue areas in **d** and **f** represent HFD home cage availability. B, baseline; WD, withdrawal. All error bars represent s.e.m. $^{*}P < 0.05$, $^{**}P < 0.01$, $^{***}P < 0.001$ and $^{****}P < 0.0001$.

HFD exposure. Indeed, although systemic ghrelin injection consistently stimulated ARC^{AgRP} neurons in mice maintained on SD, HFD-treated animals exhibited an impaired ARC^{AgRP} response to ghrelin (Fig. 4e–h), consistent with a model of HFD-induced ghrelin resistance[36,37]. However, after a 2-week HFD withdrawal, ARC^{AgRP} responses to ghrelin were not significantly different from baseline. Interestingly, although within-group deficits in ghrelin-evoked ARC^{AgRP} activity did not reach significance until 8 weeks of diet exposure, there was a significant correlation between HFD-induced weight gain and diminished ghrelin-evoked ARC^{AgRP}

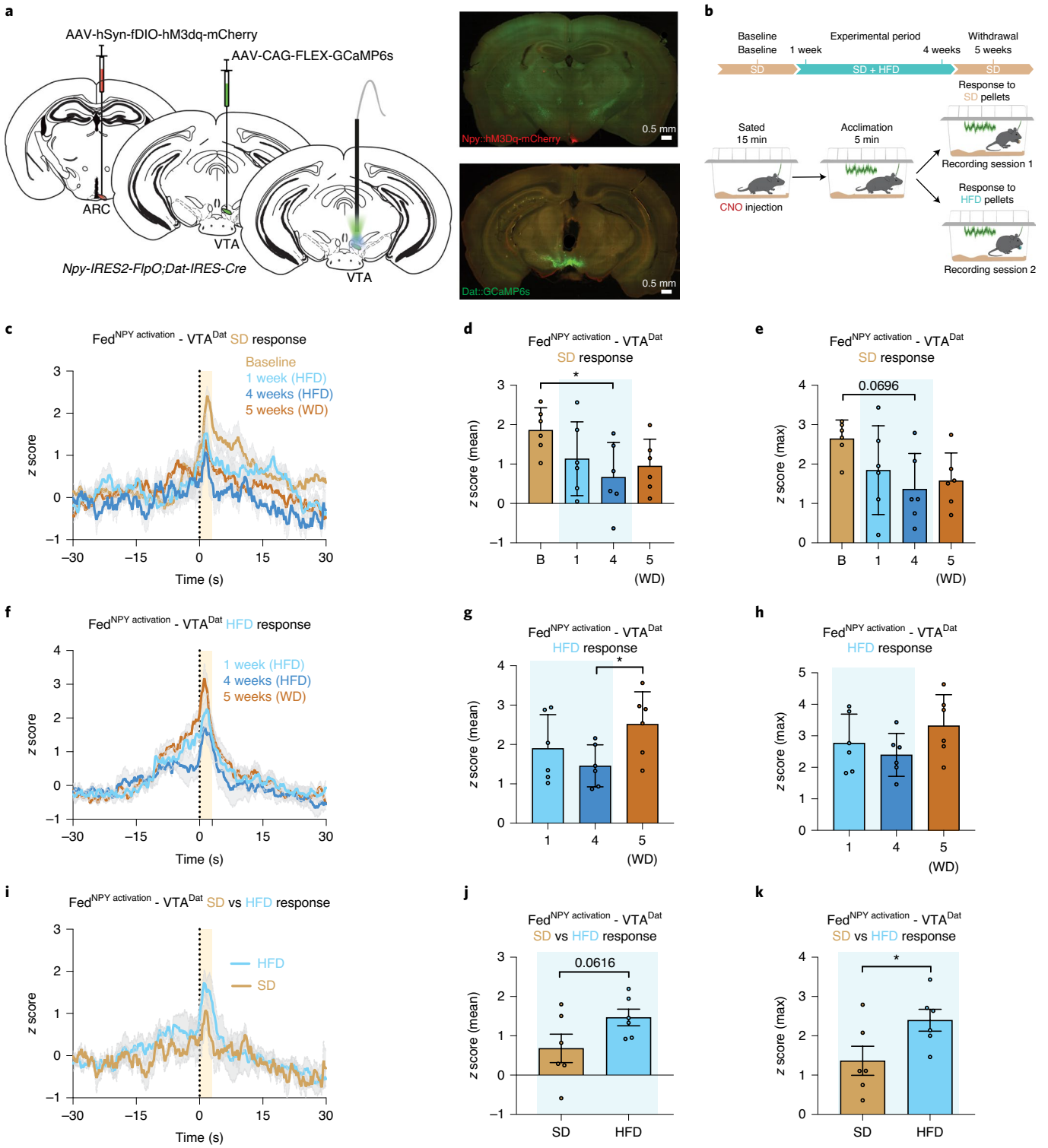

Fig. 6 | HFD alters ARC^{Npy}-mediated VTA^{Dat} responses to SD. a, Left: brain schematic of unilateral viral delivery of Flp-inducible hM3Dq and Cre-inducible GCaMP6s to the ARC and VTA, respectively, of Npy-ires2-FlpO;Dat-ires-Cre mice and optical fiber implant. Right: representative image of Npy::hM3dq (top) and Dat::GCaMP6s (bottom) expression. **b**, Experimental timeline and group schematic for fed photometry recordings. **c**,**f**, Averaged *z*-score traces of VTA^{Dat} activity aligned to (**c**) SD or (**f**) HFD pellet consumption across recording weeks. **d**,**e**,**g**,**h**, Within-subject comparisons of (**d**,**g**) mean and (**e**,**h**) maximum fluorescence *z* score during (**d**,**e**) SD ($n=6$, males and females, repeated-measures one-way ANOVA, time: $F_{3,15}=3.538$, $P=0.0407$(**d**); time: $F_{3,15}=2.802$, $P=0.0757$, Tukey's multiple comparisons (**e**)) or (**g**,**h**) HFD pellet consumption across sessions ($n=6$, males and females, repeated-measures one-way ANOVA, time: $F_{2,10}=4.073$, $P=0.0508$ (**g**); time: $F_{2,10}=2.454$, $P=0.1358$, Tukey's multiple comparisons (**h**)). **i**, Comparison of averaged *z*-score traces of VTA^{Dat} activity aligned to SD or HFD pellet consumption at 4 weeks. **j**,**k**, Within-subject comparisons of (**j**) mean ($n=6$, males and females, paired *t*-test (two tailed), $P=0.0616$) and (**k**) maximum fluorescence *z* score comparing SD and HFD pellet consumption at 4 weeks ($n=6$, males and females, paired *t*-test (two tailed), $P=0.042$). B, baseline; WD, withdrawal. Shaded peach regions in **c**, **f** and **i** represent quantified pellet retrieval period. Shaded blue areas in **d**, **e**, **g**, **h**, **j** and **k** represent HFD home cage availability. Time 0 denotes consumption. All error bars and shaded regions of **c**, **f** and **i** represent s.e.m. *$P<0.05$.

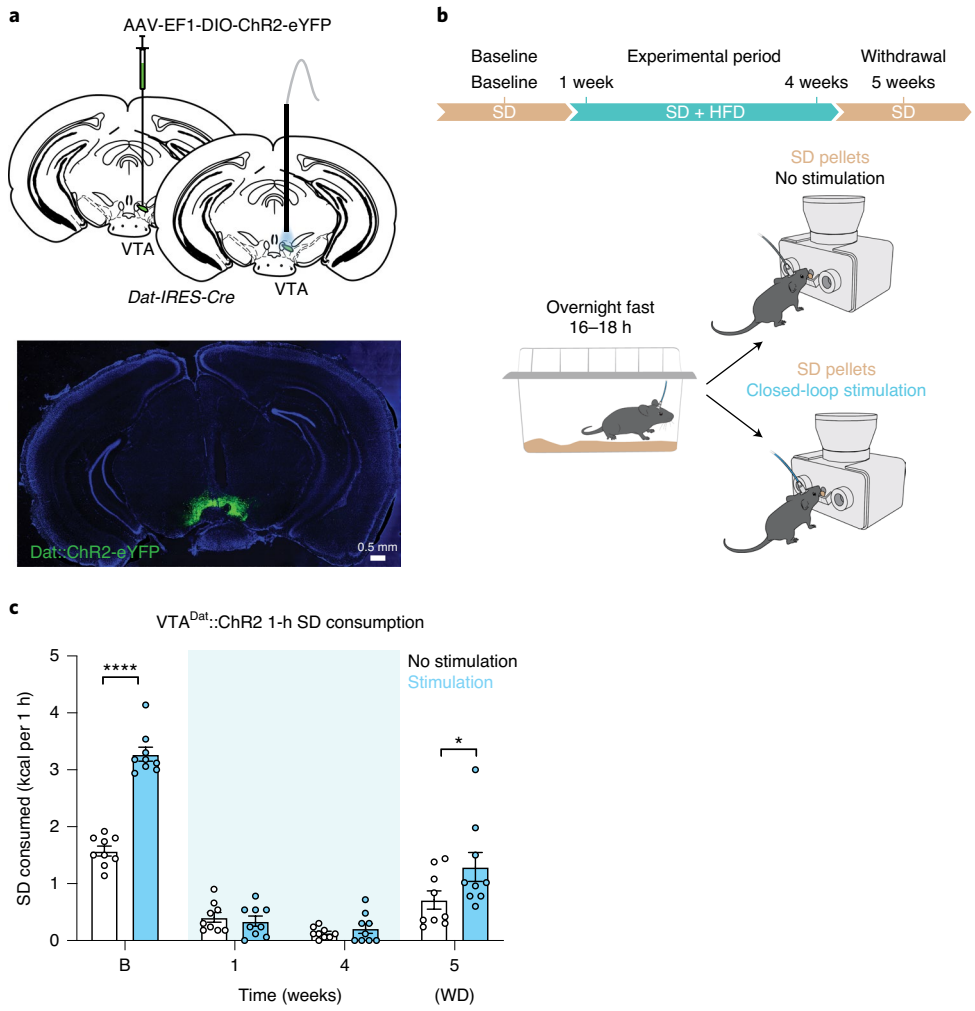

Fig. 7 | HFD exposure disrupts functional capacity of VTA^{Dat} neurons to potentiate SD consumption. a, Left: brain schematic of unilateral viral delivery of Cre-inducible ChR2-eYFP to the VTA of Dat-ires-Cre mice and optical fiber implant. Right: representative image of ChR2-eYFP expression. **b**, Experimental timeline and group schematic for closed-loop optogenetic studies with or without light stimulation. **c**, Within-subject comparison of 1-h SD consumption across testing sessions with or without VTA^{Dat} photostimulation ($n = 9$, males, repeated-measures two-way ANOVA, time × condition: $F_{3,48} = 18.30$, $P < 0.0001$, Bonferroni's multiple comparisons test). B, baseline; WD, withdrawal. Shaded blue area in **c** represents HFD home cage availability. All error bars represent s.e.m. *$P < 0.05$ and ****$P < 0.0001$.

activity in HFD-exposed mice at 1 and 4 weeks after HFD consumption (Extended Data Fig. 6b,c). This correlation no longer existed by 8 weeks of HFD, but it returned during the withdrawal period, in agreement with previous studies demonstrating body weight influence on ghrelin resistance (Extended Data Fig. 6d,e)[37].

As previously reported[10,11], we found that systemic administration of the gastrointestinal satiety signals cholecystokinin (CCK), serotonin (5-HT) or peptide YY (PYY) inhibits ARC^{AgRP} neurons over two baseline sessions while mice were maintained on SD (Fig. 4j–o and Extended Data Fig. 6l–q). Mice were then maintained on SD or supplied HFD access. Although all mice that were provided HFD rapidly gained weight, ARC^{AgRP} responses to all tested satiety signals remained intact through 4 weeks of HFD consumption (Fig. 4k, j–o). Furthermore, individual changes in satiety signal responses did not correlate with HFD-induced weight gain (Extended Data Fig. 6f–k). In summary, HFD exposure rapidly remodeled and impaired ARC^{AgRP} population dynamics in a manner uncoupled from sensory food detection.

HFD impairs ARC^{AgRP}-mediated SD feeding. To determine how HFD exposure affects the functionality of ARC^{AgRP}-evoked food intake, we optogenetically photoactivated ARC^{AgRP} neurons using ChR2 in mixed-sex animals (Fig. 5a–c). Slice recordings revealed no overt differences in ARC$^{AgRP::ChR2}$ neurons from mice on SD versus SD + HFD diet (Fig. 5b). One-hour SD consumption was measured longitudinally in fed animals near the onset of the light cycle before, during and after HFD challenge (Fig. 5c). As an additional control, HFD-naive mice were assessed over the same timeframe and showed consistent ARC^{AgRP}-induced feeding of SD across time (Fig. 5d and Extended Data Fig. 7a). Conversely, HFD-exposed mice had significantly reduced stimulation-induced feeding of SD compared to both their baseline response and HFD-naive animals at identical time points (Fig. 5d and Extended Data Fig. 7a). This devaluation was independent of body weight gain over the experimental period (Extended Data Fig. 7b). Consistent with physiological hunger (Fig. 1f), SD devaluation remained after 2-week HFD withdrawal (Fig. 5d and Extended Data Fig. 7a). To assess whether the observed changes in ARC^{AgRP}-evoked feeding were representative of food preference and not a generalized reduction in hunger drive, we repeated the optogenetic experiments in the HFD-exposed group in the presence of both SD and HFD (Fig. 5e). Similarly to natural hunger (Fig. 1h), ARC^{AgRP} photoactivation promoted targeted

feeding of HFD over SD, and this effect was further augmented after a 2-week HFD withdrawal period (Fig. 5f and Extended Data Fig. 7c). Therefore, HFD-induced changes in ARC^{AgRP} function are severe enough to thwart SD consumption and selectively promote HFD consumption. Furthermore, these findings suggest that SD devaluation might be compromised in downstream or parallel neural networks involved in food consumption.

HFD diminishes mesolimbic DA responses to SD. Mesolimbic DA is known to regulate food preference and valuation, and DA release can be altered by obesity[24,25,38,39]. To evaluate putative, direct input from ARC^{AgRP} neurons to the VTA, we employed a combination of anterograde tracing and slice connectivity experiments. Targeting synaptophysin expression to ARC^{AgRP} neurons (Extended Data Fig. 8a,b) revealed dense projections to the paraventricular nucleus of the hypothalamus (PVH) but few terminals in the vicinity of tyrosine hydroxylase (TH)-positive cells of the VTA (Extended Data Fig. 8c,d). ChR2-assisted circuit mapping affirmed monosynaptic connectivity to the PVH[40], whereas 0 of 45 VTA neurons recorded exhibited time-locked inhibitory post-synaptic currents (Extended Data Fig. 8e–g). To assess potential, indirect communication between ARC^{AgRP}→VTA^{Dat} neurons in vivo, as well as to determine if devaluation of SD after HFD exposure is encoded in the midbrain, we simultaneously transduced ARC^{Npy} and VTA^{Dat} neurons with the chemogenetic actuator hM3dq[41,42] and calcium indicator GCaMP6, respectively (Fig. 6a). Owing to endogenous expression of ARC$^{Dat/TH}$ neurons (Extended Data Fig. 8h), we used a Flp-dependent strategy to selectively target hM3Dq to ARC^{Npy} cells. Clozapine-N-oxide (CNO)-induced ARC^{Npy} activation rapidly drove SD intake in fed animals compared to saline vehicle injections (Extended Data Fig. 8i). Supporting our slice analyses, acute stimulation of ARC^{Npy} neurons failed to alter basal activity of VTA^{Dat} neurons (Extended Data Fig. 8j,k). Instead, we found that ARC^{Npy} activation potentiated VTA^{Dat} activity toward SD presentation (Extended Data Fig. 8l–n).

To assess whether this ARC^{Npy}-evoked response to SD was devalued after HFD exposure, we longitudinally recorded VTA^{Dat} activity in response to either SD or HFD pellets in animals before, during and after HFD challenge (Fig. 6b). Baseline recordings before HFD challenge demonstrated that increased VTA^{Dat} responses aligned to SD consumption, effects that were diminished after HFD exposure (Fig. 6c–e). The response to HFD pellets remained similar throughout HFD challenge, with a potentiation in the response after withdrawal (Fig. 6f–h). Critically, after 4-week HFD challenge, the response to HFD pellets elicited a stronger VTA^{Dat} response than SD pellets (Fig. 6i–k).

VTA^{Dat} stimulation is highly rewarding and leads to real-time place preference (Extended Data Fig. 9a–c)[43]. ChR2 was selectively expressed in VTA^{Dat} neurons, and SD consumption was measured longitudinally before, during and after HFD exposure in fasted animals with or without light stimulation (Fig. 7a,b). As we found VTA^{Dat} activity ramped up at the time of pellet retrieval (Fig. 6d–f), we transiently photoactivated VTA^{Dat} neurons as animals removed an SD pellet from the feeding device (Fig. 7b). We found that VTA^{Dat} activation during pellet retrieval enhanced SD consumption in fasted, HFD-naive mice at baseline (Fig. 7c). HFD exposure strongly suppressed fasting-induced consumption of SD, even when pellet retrieval was paired with VTA^{Dat} stimulation (Fig. 7c and Extended Data Fig. 9d). Although SD devaluation remained after a 1-week HFD withdrawal period, VTA^{Dat} photoactivation upon SD pellet retrieval lowered this devaluation (Fig. 7c and Extended Data Fig. 9d), suggesting that this potentiation is reversible.

To pinpoint a downstream node contributing to SD devaluation, we longitudinally assessed DA release in the shell of the nucleus accumbens (AcbSh) using the DA optical sensor GRAB-DA2m in fasted mice in response to either SD or HFD pellets (Fig. 8a,b)[44]. Reinforcing our ARC^{Npy}-evoked VTA^{Dat} recordings above, DA release during SD pellet approach and retrieval was bolstered in fasted versus fed animals (Extended Data Fig. 10a–c). After 1 week of HFD access, SD approach and retrieval resulted in reduced DA release compared to baseline (Fig. 8c–e). Critically, DA release to SD remained consistent over time in HFD-naive mice (Extended Data Fig. 10d–f). This DA-evoked devaluation of SD persisted throughout HFD exposure and started to approach baseline levels after HFD withdrawal (Fig. 8c–e). DA release in response to HFD pellets remained similar across time in the same animals that exhibited SD devaluation (Fig. 8f–h). Supporting the notion that DA shapes the value of food, HFD-exposed animals demonstrated a larger response to HFD versus SD pellet approach and retrieval at 1 week of HFD challenge (Fig. 8i–k). Collectively, these data demonstrate a robust plasticity in multiple neural circuits that contributes to food devaluation, helping explain the challenges of dieting in an obesogenic environment.

Discussion

Despite an ever-expanding number of new diets, many people who are successful in adopting healthier lifestyles often return to old eating habits. Here we reveal fatty-food-altered responsivity and functional drive of ARC^{AgRP} and VTA^{Dat} neurons toward SD, corresponding with devaluation that persists despite HFD removal, a condition analogous to a strict diet. These chronic and recalcitrant circuit adaptations illuminate the underlying difficulty in dieting as hypothalamic and mesolimbic neural circuits, encoding negative and positive affective states, respectively, now produce a sustained multifaceted tuning toward calorically dense food.

Homeostatic food seeking is generated by ARC^{AgRP} neurons through an interoceptive negative valence signal that is relieved by sensory detection of food and subsequent consumption[12]. We observed that HFD challenge diminishes ARC^{AgRP} neuron responses to SD both before and after consumption, thus preventing alleviation of the negative valence signal and promoting continued seeking of an alternative food source. Similarly, ARC^{AgRP} neuron responses to peripheral nutritional status were impaired even when an equal

Fig. 8 | HFD exposure dampens AcbSh DA release in response to SD. a, Left: brain schematic of unilateral viral delivery of the DA sensor GRAB-DA2m and tdTomato to the AcbSh and optical fiber implant. Right: representative image of GRAB-DA2m and tdTomato expression in the AcbSh. **b**, Experimental timeline and group schematic for photometry recordings. **c**,**f** Averaged *z*-score traces of DA2m fluorescence aligned to (**c**) SD or (**f**) HFD pellet retrieval across recording weeks. **d**,**e**,**g**,**h**, Within-subject comparisons of (**d**,**g**) mean and (**e**,**h**) maximum fluorescence *z* score during (**d**,**e**) SD ($n = 7$–8, males and females, mixed-effects model, time: $F_{1.555,9.847} = 11.91$, $P = 0.0034$(**d**); time: $F_{1.599,10.12} = 6.608$, $P = 0.0182$, Tukey's multiple comparison (**e**)) or (**g**,**h**) HFD pellet consumption across sessions ($n = 7$–8, males and females, mixed-effects model, time: $F_{1.950,11.70} = 0.2897$, $P = 0.7484$ (**g**); time: $F_{1.832,10.99} = 0.8452$, $P = 0.4461$ (**h**)). **i**, Comparison of averaged *z*-score traces of DA2m fluorescence aligned to SD or HFD pellet consumption at 1 week. **j**,**k**, Within-subject comparisons of (**j**) mean ($n = 8$, males and females, paired *t*-test (two tailed), $P = 0.021$) and (**k**) maximum fluorescence *z* score comparing SD and HFD pellet consumption at 1 week ($n = 8$, males and females, paired *t*-test (two tailed), $P = 0.0578$). Shaded peach and blue regions in **c**, **f** and **i** represent quantified pellet approach and retrieval period. Shaded blue areas in **d**, **e**, **g**, **h**, **j** and **k** represent HFD home cage availability. B, baseline; WD, withdrawal. Time 0 denotes consumption. All error bars and shaded regions of **c**, **f** and **i** represent s.e.m. $^*P < 0.05$ and $^{**}P < 0.01$.

caloric load was directly infused into the stomach, suggesting that a history of HFD consumption might set a steeper caloric requirement to fully alleviate ARC^{AgRP} activity. These findings underlie a developing disconnect between functional ARC^{AgRP} responses to signals of hunger and satiety and actual caloric content. Upstream neural adaptations might play a role as well, as demonstrated by HFD-induced alterations in DMH^{LepR} responses to food and pre-synaptic release. Notably, re-exposure to HFD after withdrawal induced robust feeding and stronger inhibition of ARC^{AgRP} neurons under conditions of satiety, providing an avenue for ARC^{AgRP} neurons to promote binge-like consumption during dietary relapse even in the absence of hunger.

A caveat of fiber photometry recordings is the inability to resolve individual cellular activity. Although calcium recordings of ARC^{AgRP} activity demonstrate homogenous responses to food[12], in vivo electrical recordings[8] and projection-specific activation studies[45] suggest potential heterogeneity that cannot be captured with this technique. Nonetheless, our spectrum-based approach is optimized

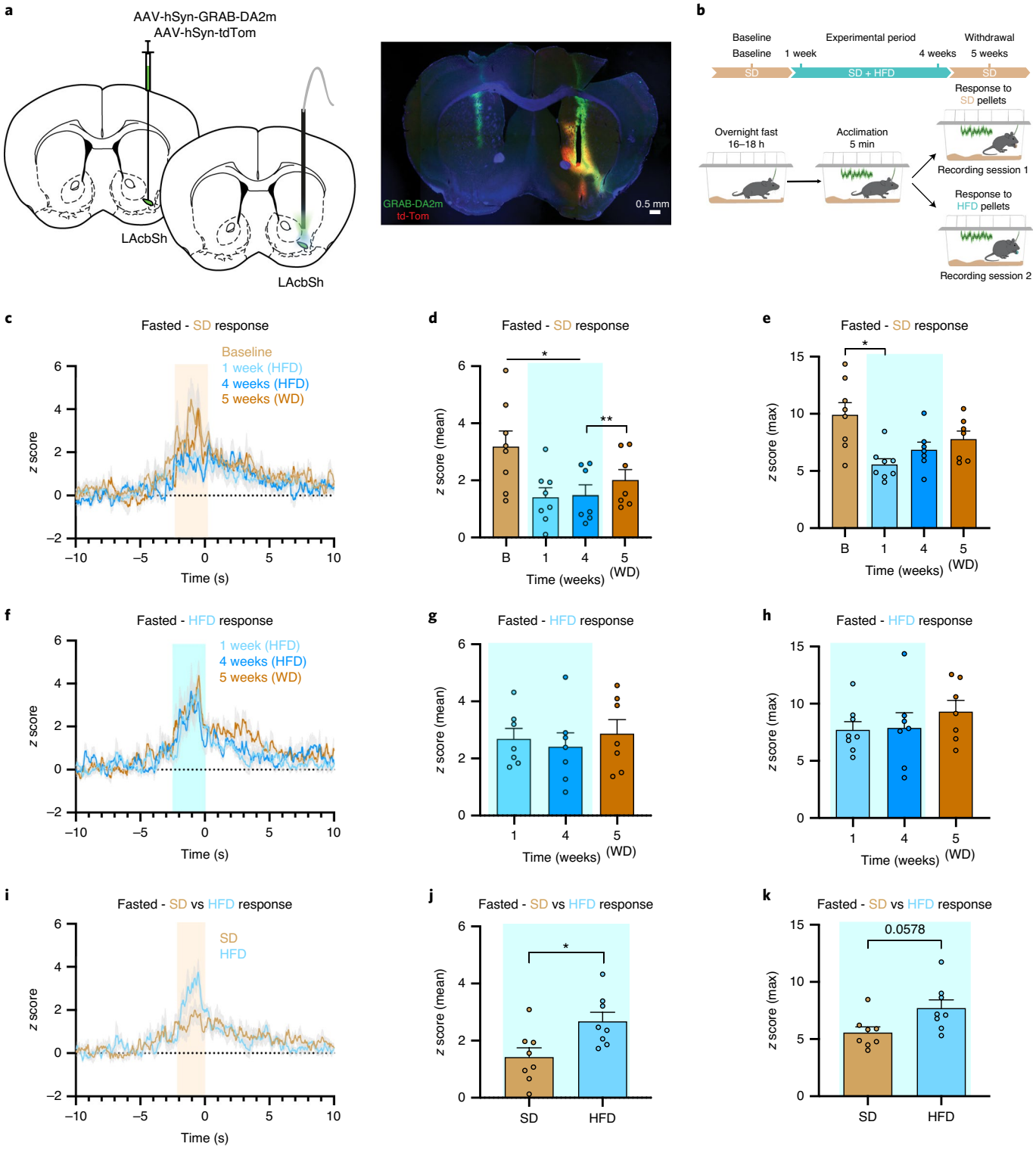

for longitudinal recordings to control for changes in GCaMP6 expression over time and HFD-induced inflammation[1]. This approach enabled the discovery that HFD exposure significantly diminishes basal ARC^{AgRP} activity. Interestingly, acute alcohol and non-nutritive drugs lead to ARC^{AgRP} inhibition[17], perhaps implicating a common mechanism through which prolonged exposure to drugs of abuse, including HFD, can negatively shift ARC^{AgRP} basal activity. Localizing the sources contributing to this depression will be subject to future studies.

In addition to homeostatic eating, we observed changes in hedonic drive as reflected by changes in mesolimbic DA signaling. Although we observed no evidence of direct communication between ARC^{AgRP}→VTA^{Dat} neurons, we report that both physiological and artificial hunger potentiate DA signaling to food[17]. The HFD-induced devaluation of SD observed in the DA system described here aligns with previous work exhibiting changes in basal midbrain DA activity, projections and release after palatable diet exposure[19,25,46,47]. Going forward, it will be important to determine whether DA accumbal signaling loses reinforcement properties independent of food discovery after HFD exposure. Interestingly, the magnitude of the DA response to HFD was similar to the response to SD before HFD exposure, possibly suggesting that HFD had displaced the value of SD for fasting-induced motivated feeding. Of note, activity of dorsal and ventral striatal circuits can reflect nutritional and hedonic value of food, respectively[39,47]. Although imaging studies have not been performed in adult human patients naive to fatty food, our findings are similar to enhanced striatal DA activity observed in obese individuals presented with images of calorically dense food[20–22]. Studies in human patients further showed diminished striatal function during food consumption and weight gain and were tied to deficits in D2R expression[48,49]. Critically, our work relies on a D2R-mimicking DA sensor and allows us to detect DA release independent of endogenous D2 availability. Together, our observed functional alterations in homeostatic and hedonic circuits provide a mechanistic blueprint for the obstinate challenges associated with dieting in an environment filled with energy-rich foods.

Online content

Any methods, additional references, Nature Research reporting summaries, source data, extended data, supplementary information, acknowledgements, peer review information; details of author contributions and competing interests; and statements of data and code availability are available at https://doi.org/10.1038/s41593-020-0684-9.

Received: 10 December 2019; Accepted: 30 June 2020;
Published online: 03 August 2020

References

1. Timper, K. & Brüning, J. C. Hypothalamic circuits regulating appetite and energy homeostasis: pathways to obesity. *Dis. Model. Mech.* **10**, 679–689 (2017).
2. DiFeliceantonio, A. G. & Small, D. M. Dopamine and diet-induced obesity. *Nat. Neurosci.* **22**, 1–2 (2019).
3. Ferrario, C. R. et al. Homeostasis meets motivation in the battle to control food intake. *J. Neurosci.* **36**, 11469–11481 (2016).
4. Luquet, S., Perez, F. A., Hnasko, T. S. & Palmiter, R. D. NPY/AgRP neurons are essential for feeding in adult mice but can be ablated in neonates. *Science* **310**, 683–685 (2005).
5. Aponte, Y., Atasoy, D. & Sternson, S. M. AGRP neurons are sufficient to orchestrate feeding behavior rapidly and without training. *Nat. Neurosci.* **14**, 351–355 (2011).
6. Krashes, M. J. et al. Rapid, reversible activation of AgRP neurons drives feeding behavior in mice. *J. Clin. Invest.* **121**, 1424–1428 (2011).
7. Takahashi, K. A. & Cone, R. D. Fasting induces a large, leptin-dependent increase in the intrinsic action potential frequency of orexigenic arcuate nucleus neuropeptide y/agouti-related protein neurons. *Endocrinology* **146**, 1043–1047 (2005).
8. Mandelblat-Cerf, Y. et al. Arcuate hypothalamic AgRP and putative pomc neurons show opposite changes in spiking across multiple timescales. *eLife* **4**, 1–25 (2015).
9. Chen, Y., Lin, Y.-C., Kuo, T.-W. & Knight, Z. A. Sensory detection of food rapidly modulates arcuate feeding circuits. *Cell* **160**, 829–841 (2015).
10. Beutler, L. R. et al. Dynamics of gut–brain communication underlying hunger. *Neuron* **96**, 461–475 (2017).
11. Su, Z., Alhadeff, A. L. & Betley, J. N. Nutritive, post-ingestive signals are the primary regulators of AgRP neuron activity. *Cell Rep.* **21**, 2724–2736 (2017).
12. Betley, J. N. et al. Neurons for hunger and thirst transmit a negative-valence teaching signal. *Nature* **521**, 180–185 (2015).
13. Baver, S. B. et al. Leptin modulates the intrinsic excitability of AgRP/NPY neurons in the arcuate nucleus of the hypothalamus. *J. Neurosci.* **34**, 5486–5496 (2014).
14. Salamone, J. D., Correa, M., Mingote, S. & Weber, S. M. Nucleus accumbens dopamine and the regulation of effort in food-seeking behavior: implications for studies of natural motivation, psychiatry, and drug abuse. *J. Pharmacol. Exp. Ther.* **305**, 1–8 (2003).
15. Berridge, K. C. 'Liking' and 'wanting' food rewards: brain substrates and roles in eating disorders. *Physiol. Behav.* **97**, 537–550 (2009).
16. Wise, R. A. Role of brain dopamine in food reward and reinforcement. *Philos. Trans. R. Soc. B Biol. Sci.* **361**, 1149–1158 (2006).
17. Alhadeff, A. L. et al. Natural and drug rewards engage distinct pathways that converge on coordinated hypothalamic and reward circuits. *Neuron* **103**, 891–908.e6 (2019).
18. Denis, R. G. P. et al. Palatability can drive feeding independent of AgRP neurons. *Cell Metab.* **22**, 646–657 (2015).
19. Fordahl, S. C. & Jones, S. R. High-fat-diet-induced deficits in dopamine terminal function are reversed by restoring insulin signaling. *ACS Chem. Neurosci.* **8**, 290–299 (2017).
20. Rothemund, Y. et al. Differential activation of the dorsal striatum by high-calorie visual food stimuli in obese individuals. *Neuroimage* **37**, 410–421 (2007).
21. Stice, E., Spoor, S., Bohon, C., Veldhuizen, M. G. & Small, D. M. Relation of reward from food intake and anticipated food intake to obesity: a functional magnetic resonance imaging study. *J. Abnorm. Psychol.* **117**, 924–935 (2008).
22. Thanarajah, S. E. et al. Food intake recruits orosensory and post-ingestive dopaminergic circuits to affect eating desire in humans. *Cell Metab.* **29**, 695–706 (2019).
23. Ravussin, Y. et al. Effects of chronic weight perturbation on energy homeostasis and brain structure in mice. *Am. J. Physiol. Integr. Comp. Physiol.* **300**, R1352–R1362 (2011).
24. Johnson, P. M. & Kenny, P. J. Dopamine D2 receptors in addiction-like reward dysfunction and compulsive eating in obese rats. *Nat. Neurosci.* **13**, 635–641 (2010).
25. Cone, J. J., Chartoff, E. H., Potter, D. N., Ebner, S. R. & Roitman, M. F. Prolonged high fat diet reduces dopamine reuptake without altering DAT gene expression. *PLoS ONE* **8**, e58251 (2013).
26. Drewnowski, A. & Greenwood, M. R. C. Cream and sugar: human preferences for high-fat foods. *Physiol. Behav.* **30**, 629–633 (1983).
27. Yang, Y. Jr, D. L, S., Keating, K. D., Allison, D. B. & Nagy, T. R. Variations in body weight, food intake and body composition after long-term high-fat diet feeding in C57BL/6J mice. *Obesity* **22**, 2147–2155 (2014).
28. Guo, J., Jou, W., Gavrilova, O. & Hall, K. D. Persistent diet-induced obesity in male C57BL/6 mice resulting from temporary obesigenic diets. *PLoS ONE* **4**, e5370 (2009).
29. Carlin, J. L. et al. Removal of high-fat diet after chronic exposure drives binge behavior and dopaminergic dysregulation in female mice. *Neuroscience* **326**, 170–179 (2016).
30. Balthasar, N. et al. Divergence of melanocortin pathways in the control of food intake and energy expenditure. *Cell* **123**, 493–505 (2005).
31. Zhang, Y. et al. Positional cloning of the mouse obese gene and its human homologue. *Nature* **372**, 425–432 (1994).
32. Jais, A. & Brüning, J. C. Hypothalamic inflammation in obesity and metabolic disease. *J. Clin. Invest.* **127**, 24–32 (2017).
33. Chen, T.-W. et al. Ultrasensitive fluorescent proteins for imaging neuronal activity. *Nature* **499**, 295–300 (2013).
34. Garfield, A. S. et al. Dynamic GABAergic afferent modulation of AgRP neurons. *Nat. Neurosci.* **19**, 1628–1635 (2016).
35. Hahn, T. M., Breininger, J. F., Baskin, D. G. & Schwartz, M. W. Coexpression of Agrp and NPY in fasting-activated hypothalamic neurons. *Nat. Neurosci.* **1**, 271–272 (1998).
36. Briggs, D. I., Enriori, P. J., Lemus, M. B., Cowley, M. A. & Andrews, Z. B. Diet-induced obesity causes ghrelin resistance in arcuate NPY/AgRP neurons. *Endocrinology* **151**, 4745–4755 (2010).
37. Briggs, D. I. et al. Calorie-restricted weight loss reverses high-fat diet-induced ghrelin resistance, which contributes to rebound weight gain in a ghrelin-dependent manner. *Endocrinology* **154**, 709–717 (2013).

38. Liu, S. et al. Consumption of palatable food primes food approach behavior by rapidly increasing synaptic density in the VTA. *Proc. Natl Acad. Sci. USA* **113**, 2520–2525 (2016).
39. Roitman, M. F., Stuber, G. D., Phillips, P. E. M., Wightman, R. M. & Carelli, R. M. Dopamine operates as a subsecond modulator of food seeking. *J. Neurosci.* **24**, 1265–1271 (2004).
40. Atasoy, D., Aponte, Y., Su, H. H. & Sternson, S. M. A FLEX switch targets channelrhodopsin-2 to multiple cell types for imaging and long-range circuit mapping. *J. Neurosci.* **28**, 7025–7030 (2008).
41. Armbruster, B. N., Li, X., Pausch, M. H., Herlitze, S. & Roth, B. L. Evolving the lock to fit the key to create a family of G protein-coupled receptors potently activated by an inert ligand. *Proc. Natl Acad. Sci. USA* **104**, 5163–5168 (2007).
42. Alexander, G. M. et al. Remote control of neuronal activity in transgenic mice expressing evolved G protein-coupled receptors. *Neuron* **63**, 27–39 (2009).
43. Tsai, H.-C. et al. Phasic firing in dopaminergic neurons is sufficient for behavioral conditioning. *Science* **324**, 1080–1084 (2009).
44. Sun, F. et al. A genetically encoded fluorescent sensor enables rapid and specific detection of dopamine in flies, fish, and mice. *Cell* **174**, 481–496 (2018).
45. Betley, J. N., Cao, Z. F. H., Ritola, K. D. & Sternson, S. M. Parallel, redundant circuit organization for homeostatic control of feeding behavior. *Cell* **155**, 1337–1350 (2013).
46. Lippert, R. N. et al. Maternal high-fat diet during lactation reprograms the dopaminergic circuitry in mice. *J. Clin. Invest.* **130**, 3761–3776 (2020).
47. Tellez, L. A. et al. Separate circuitries encode the hedonic and nutritional values of sugar. *Nat. Neurosci.* **19**, 465–470 (2016).
48. Stice, E., Yokum, S., Blum, K. & Bohon, C. Weight gain is associated with reduced striatal response to palatable food. *J. Neurosci.* **30**, 13105–13109 (2010).
49. Volkow, N. D., Wang, G.-J. & Baler, R. D. Reward, dopamine and the control of food intake: implications for obesity. *Trends Cogn. Sci.* **15**, 37–46 (2011).

Methods

Animals. C57BL/6J mice, *Agrp*$^{tm1(cre)Lowl}$/J (stock no. 012899), B6.SJL-*Slc6a3*$^{tm1.1(cre)Bkmn}$/J (stock no. 006660), B6;129S4-*Mc4r*^{tm1Lowl}/J (stock no. 006414), B6.Cg-*Lep*^{ob}/J (stock no. 000632) and *LepRb*$^{(cre)}$ mice were used. Mice were housed with a 12-h light/dark cycle with ad libitum access to water and standard chow (Envigo 7017 NIH-31, 14% kcal from fat) unless otherwise stated. In some cases, *Agrp*$^{tm1(cre)Lowl}$ were crossed with B6.Cg-*Gt(ROSA)26Sor*$^{tm9(CAG-tdTomato)Hze}$/J (stock no. 007909)[50] to generate AgRP-Ai9 reporter mice for use with spectrometer-based in vivo fiber photometry recordings. *LepRb*$^{(cre)}$ mice were crossed with *B6.FVB-Tg(Npy-hrGFP)1Lowl/J* (stock no. 006417) and *Agrp*$^{tm1(cre)Lowl}$ were crossed with *B6;129S-Gt(ROSA)26Sor*$^{tm32(CAG-COP4*H134R/EYFP)Hze}$/J (stock no. 012569) to generate mice for ephys studies. B6.Cg-*Npy*$^{tm1.1(flpo)Hze}$/J (stock no. 030211) mice were crossed with B6.SJL-*Slc6a3*$^{tm1.1(cre)Bkmn}$/J (stock no. 006660) for combinatorial chemogenetic and photometric recordings. All animal protocols and procedures were approved by the US National Institute of Environmental Health Sciences Animal Care and Use Committee or the National Institutes of Health Animal Care and Use Committee. Mice were group housed before the start of experiments and were transferred to single housing after stereotaxic surgery or during home cage feeding measures. After baseline recordings where mice had ad libitum access to water and standard chow, a select group was put on ad libitum access to water, standard chow and high-fat diet (Research Diets D12492, 60% kcal from fat) for the duration of the experimental period. During the withdrawal period, all mice had ad libitum access to water and standard chow. All experiments were carried out in adult (>8 weeks) male and female mice with the exception of optogenetic stimulation of VTA^{DA} neurons, which used only males.

Viral vectors. AAV1-hsyn-FLEX-GCaMP6s (Addgene, v100845) was used for spectrometer-based fiber photometry recordings of AgRP-positive ARC neurons and recordings of DAT-positive VTA neurons. For DA sensor recordings, AAV9-hsyn-GRAB-DA2m (Vigene Biosciences) was mixed with AAV9-hsyn-tdTomato (NIEHS Viral Vector Core) at a ratio of 5:1 before injection. AAVrh10-CAGGS-FLEX-ChR2-tdTomato-WPRE-SV40 (Addgene, 18917) was used with optogenetic stimulation experiments to stimulate AgRP-positive neurons in the ARC and LepR-positive neural projections to the ARC. AAV5-hSyn-hChR2EYFP(H134R) (Addgene, 26973) was used with optogenetic stimulation experiments to stimulate DAT-positive neurons in the VTA. AAV1-CAG-FLEX-X-jG-GCaMP7s-WPRE (Addgene, 104495) was used with in vivo fiber photometry experiments to longitudinally record from AgRP-positive neurons in the ARC during gastric infusion. AAV5/2-hSyn-dFRT-hM3dq-mCherry (VVF University of Zurich, v189-5) was used for chemogenetic activation experiments of Npy/AgRP-positive neurons in ARC. All viruses had a titer of more than 10^{12} viral particles per milliliter.

Viral injections. Stereotaxic injections were performed as previously described[51]. Mice were anesthetized with isoflurane and placed into a stereotaxic apparatus (Kopf Instruments or Stoelting Instruments). After sterilization of the incision site with ethanol and betadine, the skull was exposed via a small incision. Small burr holes were drilled above the microinjection target sites. A 2-µl Neuros Hamilton Syringe with a 30-gauge needle was used to microinject virus into the target sites at a rate of 100 nl min^{-1} using a syringe pump (World Precision Instruments). The needle was slowly withdrawn 5 min after the completion of the injection to reduce backflow of the virus. Target coordinates relative to bregma (in mm) and viral volumes injected were as follows: ARC (AP: −1.50 to −1.55, ML: ± 0.30, DV: −5.85, 700 nl per side); AcbSh (AP: 1.00, ML: ± 1.70 to 2.00, DV: −4.40 to −4.60, 400 nl per side). After surgery, the incision was closed using surgical sutures. In some cases, viral injections were performed using a pulled glass pipette, as previously described[6]. In these cases, the following coordinates were used: ARC coordinates: AP −1.45 mm, ML ± 0.25 mm, DV −5.75 mm and −5.65 mm (300 nl per side); VTA coordinates: AP −3.05 mm, ML ± 0.35 mm, DV −4.45 mm and −4.25 mm (150 nl unilaterally); DMH coordinates: AP −1.80 mm, ML ± 0.30 mm, DV −5.2 mm.

Intragastric catheter implantation. *Agrp-IRES-Cre* mice that were already implanted with an optical fiber were anesthetized with isoflurane. Abdominal midline incisions were made through the skin and muscle layers separately. Then, 8-mm gastric catheters made of Micro-Renathane tubing with epoxy balls on each end (Braintree Scientific, MRE-033, 0.033 × 0.014 inches) were implanted in the fundus and secured with surgical mesh (Bard, 0112660) glued with liquid adhesive (Devcon Clear Epoxy Adhesive, 92926). This procedure was adopted from previous work[11]. The abdominal layer was stitched with Coated Vicryl Violet Braided Sutures 5–0 (Ethicon, J385H), whereas the skin layer was closed with 9-mm wound clips using a MikRon 9-mm autoclip applier (Braintree Scientific, 205016 and 205000). Mice were treated postoperatively with buprenorphine slow-release analgesia (1.2 mg kg^{-1} subcutaneously). Mice for gastric infusions were allowed 2 weeks from the time of catheter implantation to recover, with a periodic flush of deionized water to keep the catheter from clogging with food particles.

Drugs. Ghrelin (Tocris, 1465), CCK octapeptide (Bachem, cat. no. 4033010), PYY 3–36 (R&D Systems, cat. no. 1618) and 5-HT (Sigma-Aldrich, cat. no. H9523) were dissolved in saline at stock concentrations and stored at −80 °C until use. On the day of testing, the stock was thawed, diluted with saline and delivered at a volume of 10 ml kg^{-1} at the following doses: ghrelin (1 mg kg^{-1}), CCK (10 µg kg^{-1}), 5-HT (2 mg kg^{-1}) and PYY (0.1 mg kg^{-1}).

Spectrometer-based fiber photometry system. For in vivo fiber photometry recordings of ARC^{AgRP} neuron responses to home cage food presentation, ghrelin, gastrointestinal satiety signals and accumbal DA release with a fluorescent DA sensor, we used a spectrally resolved fiber photometry system as described previously[51]. Briefly, a laser beam from a 488-nm, 60-mW continuous wave (CW) laser (OBIS 488LS-60, Coherent) was aligned into a fluorescence cube and reflected using a dichroic mirror (ZT488/561rpc, Chroma Technology) into the core of a multimode patch cable (M72L05, Thor Labs). This patch cable was connected to an optical joint (FRJ_1×1, Doric Lenses) followed by a second patch cable that ended with an FC ceramic ferrule (200-µm core diameter, 0.39NA; M83L01, Thor Labs) This patch cable could be connected to an optical probe implanted with the mouse via coupling with a ceramic split sleeve (SM-CS125S, Precision Fiber Products). Emission was collected by the optical fiber tip and then passed through the same patch cables before passing through the dichroic of the filter cube. Here, the emitted light was routed into an AR-coated multi-mode patch cable connected to the entrance port of a spectrometer (QE Pro-FL, Ocean Optics). Spectral data were acquired by OceanView software (Ocean Optics). In rare cases, a 561-nm, 60-mW CW laser (OBIS 561LS-60, Coherent) was used simultaneously to increase red fluorescence emission in tdTomato. Light intensity outputs as measured at the end of the final patch cable tip were adjusted to be 50–70 µW for 488-nm excitation and 40 µW for 561-nm excitation when used.

Optical fiber implantation. For spectrometer-based fiber photometry recordings, optical fiber implants were constructed by threading an optical fiber (200 µm, 0.39 NA; FT200EMT, Thor Labs) through a ceramic ferrule with a 1.25-mm OD (MM-CON2007–2300, Precision Fiber Products) and secured with heat-cured epoxy (Epoxy 353ND, Precision Fiber Products) and then polished and cleaved to length. At least 3 weeks after viral injection surgery, mice underwent a second stereotaxic surgery to receive a unilateral implantation of the optical fiber. The optical fiber was connected to a patch cable (200 µm, 0.39NA, Thor Labs) using a ceramic split sleeve (SM-CS125S, Precision Fiber Products), which was connected to the spectrometer-based photometry system with blue (488 nm) illumination (50–70 µW). This allowed for real-time visualization of fluorescent emission signal of GCaMP and tdTomato, or DA2m and tdTomato, during probe implantation. After the mouse was anesthetized on the stereotax and the skull was exposed, a burr hole was drilled above the target site (ARC or AcbSh). The optical fiber was lowered to the ARC (GCaMP-based experiments) or lateral AcbSh (DA2m-based experiments) slowly until a maximum fluorescent signal was obtained. If no fluorescent emission signal was observed, the probe was slowly retracted, cleaned with sterile saline and lens paper and then lowered into the corresponding target structure of the opposite hemisphere. Once positioned, the optical fiber was secured to the skull using Metabond (Parkell). Mice were then placed into single housing for the remainder of experiments. Mice recovered for at least 1 week before the start of recording sessions. For fiber implantation in the ARC for photostimulation experiments: AP −1.45 mm, ML ± 0.25 mm, DV −5.40 mm. For fiber implantation in the VTA for photostimulation experiments: AP −3.05 mm, ML ± 0.35 mm, DV −4.05 mm. For fiber implantation in the ARC for in vivo photometry recordings with gastric infusions: AP −1.45 mm, ML ± 0.22 mm, DV −5.60 mm.

AgRP home cage photometry. AgRP-Ai9 mice expressing GCaMP6s in ARC^{AgRP} neurons were handled by the experimenter at least 1 week before the start of recordings. Body weights and home cage food intake were measured at least weekly. Photometry recordings were conducted during the light cycle, and mice were transferred to a new home cage the night before testing. During photometry recordings, nestlets were removed from the home cage to aid in visualization of the bedding and were returned to the home cage upon completion of the recording trial. A patch cable (detailed above) was connected to the optical fiber implant, and the home cage was placed in a sound-attenuating box with illumination from the Med Associates house light. Fluorescence spectra that included GCaMP and tdTomato were acquired using a 19-ms integration time and were triggered at 25-Hz TTL pulses sent from a digital output module (DIG-726TTL, Med Associates). A digital video camera (Grasshopper3 GS3-U3–23S6M-C, FLIR, Integrated Imaging Solutions) captured the entire home cage during recording and was triggered frame by frame by the same TTL pulses. This allowed us to match each video frame with the corresponding fluorescence signal.

ARC^{AgRP} photometry responses were tested repeatedly across three types of recording sessions: ghrelin, fed and fasted. In all conditions, mice were recorded for 15 min before either a ghrelin injection or the addition of food to the cage. For ghrelin recordings, mice received a 1-mg kg^{-1} intraperitoneal injection of ghrelin and were returned to the home cage for 5 min. During fed recordings, after the 15-min period, a pre-weighed chow pellet was added to the corner of the home cage. Recording continued for 5 min, after which a second pre-weighed chow pellet (chow group for all sessions; B1 and B2 time points for the HFD group) or HFD (HFD

group; 1 week, 4 weeks, 8 weeks and withdrawal time points) was added to the cage. The weight of the first pellet was determined at this time, and it was returned to the home cage. The recording continued for 5 min after the addition of the second pellet. Fasted recordings were identical to fed recordings with the exception that mice were food deprived beginning ~18 h before the recording session.

AgRP responses to intraperitoneal administration of the gastrointestinal satiety signals CCK (10 μg kg^{-1}), 5-HT (2 mg kg^{-1}) and PYY (0.1 mg kg^{-1}) were tested in a separate cohort of mice. Mice were fasted ~18 h before the recording sessions. To reduce the number of required overnight fasts, we tested each mouse's response to all three compounds on the same day. Recordings were separated by at least 1 h per drug per mouse and always in the order of CCK, 5-HT and then PYY, as only PYY had long-lasting inhibition of AgRP neurons. After PYY testing, mice were immediately returned to ad libitum access to their home cage diets until the next testing session, which was at least 1 week later.

AgRP home cage photometry data analysis. Raw emission spectra data were passed through a spectral linear unmixing algorithm written in R that was detailed previously[51]. To correct for motion artifacts, unmixed coefficient values for GCaMP were normalized to the unmixed coefficients for tdTomato to generate GCaMP/tdTomato ratio values that were treated as *F*. Then, %d*F*/*F* was calculated using the following formula: $(100 \times (F - F_0)/F_0)$, where F is the fluorescence ratio value of a given frame and F_0 was defined as the mean F value during the 5 min prior to when a hand entered the video frame to pick up the mouse for a drug injection or to add the first food pellet. Quantified responses to ghrelin and Pellet 1 were measured as the mean %dF/F value during the last 2 min during the 5 min after the injection or pellet addition (minutes 3–5). %dF/F changes during Pellet 2 were calculated similarly and reported as the difference from the Pellet 1 response. For photometry measurements aligned to the first bite of food, the calculated %dF/F values were aligned to the first frame of a visible feeding bout occurring within the first 5 min of pellet addition, and the average %dF/F 1 s before the bite was calculated. Sessions where mice did not consume the SD pellet during these 5 min were excluded from bite alignment analyses, which only occurred in mice from sessions after HFD exposure. For satiety signal experiments (CCK, 5-HT and PYY), the mean %dF/F value during the first 10 min after injection (minutes 0–10) and the next 10 min after injection (minutes 10–20) were averaged. Correlations between photometry measurements and body weight changes across weeks were calculated by normalizing the photometry response on a given week to the individual mouse's average across the baseline B1 and B2 sessions, whereas weight was normalized to the body weight of each mouse on the day it first received access to HFD or the matching time point for SD-only control mice.

In animals that were placed under gastric infusion experiments, no spectral unmixing algorithm was applied due to lack of tdTomato, but %dF/F was calculated using the formula: $(100 \times (F - F_0)/F_0)$ where F is the fluorescence ratio value of a given frame and F_0 was defined as the mean F value during the 5 min before the infusion. Quantified responses to infusion were measured as the mean %dF/F value during the last 2 min during the 10 min after the start of infusion (minutes 5–15) and during the last 2 min during the 10 min after pellet addition (minutes 15–25).

VTA DA home cage photometry. Npy-FlpO;DAT-cre mice expressing hM3dq in the ARC and GCaMP6s in the VTA were handled by the experimenter for 1 week before experiments, and mice were housed with a small white ramekin always present in their home cages. Experiments were conducted in the home cage at 9:00–11:00, near the beginning of the light cycle when food intake is normally low. Basal activity recordings were completed over 2 d with counterbalanced saline and CNO conditions on any given day. Mice were tethered to a patch cable, and basal activity was recorded for 5 min (baseline) before injection and for 30 min after injection. For food response recordings, the cage was changed to remove all food. Mice were then injected 30 min before recording, and their small ramekin was placed in the corner of the home cage. Food response recordings were completed over 2 d: one day being the injection of CNO with SD pellet drops, and the other day being the injection of CNO with HFD pellet drops. During the food response recordings, the experimenter dropped small SD or HFD food pellets (0.05 g each) into the ramekin. Food was not dropped if the mouse was sitting inside the ramekin.

VTA DA home cage photometry analysis. For basal activity recordings, the overall traces were fit to and subtracted by a regression line to minimize photobleaching. For food response recordings, video frames were analyzed to determine the time at which the mouse retrieved the pellet before consumption, which was defined as when the mouse had taken the pellet and assumed a stereotypical hunched posture during feeding. This was defined as time 0 for each retrieval event. The mean and maximum z scores were used for the traces, normalized to a baseline period of 60 s before each event. The normalized mean and maximum z scores for 3 s after retrieval (when observed activity is highest) were used for quantification. For each mouse, we averaged the results of the first five pellet retrievals, though the mice could retrieve up to ten pellets per session. This was done to minimize satiety-related decreases in retrieval fluorescence z scores during later pellet retrievals.

Screening protocol for chemogenetic activation experiments. Npy-IRES2-FlpO; DAT-cre mice expressing hM3dq in the ARC and GCaMP6s in the VTA were handled by the experimenter for 1 week before experiments. Screening for all Npy-IRES2-FlpO;DAT-cre mice was conducted in the home cage at 9:00–11:00, near the beginning of the light cycle when food intake is normally low, and was completed over 2 d. On any given day, injections were counterbalanced, with half of the mice receiving a saline injection and the other half receiving a CNO injection. After 30 min after injection, food was given in the home cage and measured after 30 min of access.

DA sensor photometry testing. Recordings were carried out in an open-top mouse operant chamber with a white plastic floor (21.6 × 17.8 × 12.7 cm, Med Associates) housed in a sound-attenuating box. A small petri dish was placed in a corner beneath a chute connected to a rubber tube that ran outside of the sound-attenuating box. This chute allowed for small food pellets (20–25 mg) to be dropped into the petri dish without an experimenter reaching into the box during recordings. Mice were habituated to the box with food in the dish for at least 10 min before the first testing day. Photometry recording settings and equipment were identical to those used for ARC^{AgRP} GCaMP recordings. In each recording session, mice were connected to the patch cable and placed in the testing arena for 15 min without food available in the dish. Video recording of the session began during the last 5 min of this period. After this time, the experimenter supplied one food pellet (SD or HFD depending on the session). Retrieval of the food was visualized live, and the experimenter waited at least 60 s after retrieval before the addition of another pellet. Pellets were not added if the mouse was sitting in the petri dish. Each session lasted for up to 50 min (including the 15-min period without food) or ten pellet retrievals. A maximum of four potential recording conditions were tested in a given week: Sated-Chow, Sated-HFD, Fasted-Chow and Fasted-HFD. Only one type of food was ever tested within a test session. Floors and walls of the test chamber were cleaned with 70% ethanol between mice.

DA sensor photometry analysis. Raw DA2m and tdTomato signals were unmixed using the algorithm described above. Video frames were analyzed to determine the frame in which the mouse retrieved the pellet and before consumption, which was defined as when the mouse had taken the pellet and assumed a stereotypical hunched posture during feeding. This was defined as time 0 for each retrieval event. Using custom R software, 90-s windows around each event were individually analyzed and split into four behavioral events: Baseline (−45 to −30s), Approach/Retrieval (−2 to 0 s), Consumption (1 to 6 s) and Post-Consumption (30 to 45 s). For each retrieval event, the mean and s.d. of the GCaMP/tdTomato ratio during the baseline event were calculated and used to convert each 90-s window into fluorescence z-score values. The mean z score within the behavioral windows were used for quantification. For each mouse, we averaged the results of the first five pellet retrievals, though the mice could retrieve up to ten pellets per session. This was done to minimize satiety-related decreases in Approach/Retrieval fluorescence z scores during later pellet retrievals during fasted test sessions.

In vivo photostimulation. Fiber optic cables (200-mm diameter, Doric Lenses) coupled to lasers were attached to the fiber cannula of the mice via zirconia sleeves (Doric Lenses). Light was delivered to the brain through an optical fiber (200-μm diameter core; CFMLC22U-20, Thor Labs). Light power exiting the fiber tip was 10 mW for both the ARC and VTA.

For photostimulation of AgRP-positive neurons in the ARC, pulse trains (20 Hz; 2 s on, 2 s off; 473 nm; Laserglow Technologies) were programmed using a waveform generator (PCGU100, Velleman Instruments) for continuous photostimulation during all tasks. All AgRP photostimulation experiments were conducted at 8:00–11:00, near the beginning of the light cycle when food intake is low.

For photostimulation of DAT-positive neurons in the VTA during real-time place preference, pulse trains (20 Hz, 250 ms on, 250 ms off; 473 nm; Laserglow Technologies) were custom programmed with Arduino electronics and continued for as long as the mouse remained on the side of the chamber associated with photostimulation. For photostimulation of the VTA during the fast–refeed task, pulse trains (20 Hz; 250 ms on, 250 ms off; 473 nm; Laserglow Technologies) were custom programmed with Arduino electronics and continued for 5 s after each pellet retrieval. All *DAT-Cre* mice were fasted overnight for 18 h, and photostimulation experiments were conducted at 9:00–12:00 the next morning.

Screening protocols for photostimulation. Screening for all *Agrp-IRES-Cre* mice was conducted in the home cage at 8:00–11:00, near the beginning of the light cycle when food intake is normally low. After tethering and a 20-min acclimatization period, mice were given ad libitum access to standard chow for a 20-min baseline, followed by ad libitum access to standard chow for a 20-min photostimulation period (as described). Only mice that had eaten more than 0.30 g of standard chow during the photostimulation period were selected for the experiments.

Real-time place preference (RTPP) was conducted to screen all *Dat-IRES-Cre* mice and was conducted at 9:00–12:00. The RTPP chamber was built of white plexiglass walls and floor (50 × 26 × 30 cm) with a middle partition providing equal separation of the two sides. Mice could move freely between the two sides. One side of the chamber was paired with photostimulation (as described), whereas the other side of the chamber was not. Only mice that had spent more than 55% of their time on the photostimulation side were included in the study. Movement tracking was completed using Ethovision XT 14 software (Noldus).

Food intake and weight change measurements. Male and female C57BL/6J mice had ad libitum access to water and standard chow for 10 d before they were either kept on ad libitum access to water and standard chow or put on ad libitum access to water, standard chow and high-fat diet (Research Diets D12492, 60% kcal from fat) for 8 weeks. Mice were then all kept or put on ad libitum access to water and standard chow only for 2 weeks. During this time, food intake and weights of mice were measured daily. Lean and fat mass measurements were taken weekly using quantitative magnetic resonance spectroscopy (EchoMRI 3-in-1). During fast–refeed experiments, mice were fasted overnight for 18 h and given access to either standard chow or both standard chow and high-fat diet for 1 h between 09:00 and 11:00.

Timed photostimulation during fast–refeed. All trials were conducted in a PhenoTyper (Noldus) used as a home cage and recorded and managed through Ethovision XT 14 software (Noldus). Each PhenoTyper home cage contained a Feeding Experimentation Device (FED)—an automated food dispenser[52]. FEDs dispensed 20-mg chow pellets (TestDiet) and monitored retrieval of each pellet by the mice. Mice were habituated with the FED for 3 d before testing began. All animals were fasted for 18 h and then given access to the FED for 1 h with or without stimulation. Upon retrieval of one 20-mg pellet, photostimulation at the described light pulse train lasted for 5 s, followed by an intertrial interval of 15 s during which the mouse could not retrieve another pellet.

Electrophysiology. To prepare brain slices for electrophysiological recordings, brains were removed from anesthetized mice (4–8 weeks old) and immediately submerged in ice-cold, carbogen-saturated (95% O_2 and 5% CO_2) sucrose solution (in mM): 87 NaCl, 75 sucrose, 25 glucose, 25 $NaHCO_3$, 7.5 $MgCl_2$, 2.5 KCl, 1.25 NaH_2PO_4 and 0.5 $CaCl_2$. Then, 300-µm-thick coronal sections of the arcuate nucleus were cut with a Leica VT1000S Vibratome and incubated at 32 °C in oxygenated aCSF for 60 min (in mM): 125 NaCl, 25 $NaHCO_3$, 11 glucose, 2.5 KCl, 1.25 NaH_2PO_4, 1 $MgCl_2$ and 1 $CaCl_2$ (~308 mOsm/L). Slices were maintained and recorded at room temperature (20–24 °C). For voltage–clamp recordings, intracellular solution contained the following (in mM): 70 K-gluconate, 80 KCl, 10 HEPES, 1 EGTA, 4 Na_2-ATP, 0.4 Na_2-GTP (pH 7.35) and 290 mOsm. For current–clamp recordings, intracellular solution contained the following (in mM): 130 K-gluconate, 10 KCl, 0.3 $CaCl_2$, 1 $MgCl_2$, 10 HEPES, 1 EGTA, 10 Na-phosphocreatinine, 3 Mg-ATP, 0.3 Na_2-GTP (pH 7.35) and 290 mOsm.

Light-evoked inhibitory post-synaptic currents (IPSCs) were isolated with kynurenic acid (3 mM) and recorded in the whole-cell voltage–clamp mode, with membrane potential clamped at −70 mV. All recordings were made using a Multiclamp 700B amplifier, and data were filtered at 2 kHz and digitized at 10 kHz. To photostimulate ChR2-positive fibers, a high-power white LED light source (Prizmatix) in combination with blue light filter was used. The blue light was focused onto the back aperture of the microscope objective, producing a wide field exposure. The light output was controlled by via TTL output through pClamp 10.2 software (Axon Instruments). Photostimulation-evoked IPSC paired-pulse ratio protocol comprised two blue light laser pulses (pulse duration, 2 ms) administered 200 ms apart, repeating for an average of 20 sweeps per cell. Paired-pulse ratio was calculated by peak amplitude (pulse2/pulse1). Light-evoked action potentials were recorded in the whole-cell current–clamp mode. Photostimulation of 10-ms pulse width was triggered at 10 Hz and 20 Hz.

Intragastric infusions. All trials were conducted in the home cage between 9:00 and 12:00 after an overnight fast of 18 h. Implanted gastric catheters were connected to Micro-Renathane tubing (3 feet, Braintree Scientific, MRE-033, 0.033 × 0.014 inches) and a 5-ml Luer Lock syringe placed into a pump (New Era Pump Systems, NE-1000). After a baseline period of 5 min, 1-ml infusions of either 0.9% saline or 0.86 kcal Ensure were completed over 10 min at a rate of 0.1 ml min^{-1}.

Immunohistochemical analysis. Mice were transcardially perfused with ice-cold 30 ml of phosphate-buffered saline (PBS), followed by 30 ml of 4% paraformaldehyde (PFA). Subsequently, the brains were extracted and left in 4% PFA overnight. After overnight post-fixation, the brains were transferred to PBS, from which they were coronally sectioned at 45 µm using a Leica VT1200S Vibratome. The brain slices were rinsed three times with PBS before undergoing blocking and permeabilization with 10% goat serum in 0.4% Triton-X for 1 h. They were then left to incubate overnight at 4 °C with primary antibodies diluted in PBS (1:1,000). The primary antibodies used were chicken anti-GFP (ab13970, Abcam) for detecting GCaMP6s and rabbit anti-RFP (ab62341, Abcam) for detecting tdTomato. For the nucleus accumbens samples, anti-RFP antibodies were not used owing to there being profuse tdTomato expression after viral injection. On the next day, the slices were rinsed three times with PBS and incubated in secondary antibodies diluted in PBS (1:500) for 1 h. The secondary antibodies used were Alexa Fluor 488-conjugated goat anti-chicken (A11039, Invitrogen) and Alexa Fluor 568-conjugated goat anti-rabbit (A11011, Invitrogen). After three washes with PBS, the brain slices were mounted on slides and coverslipped with VECTASHIELD HardSet Antifade Mounting Medium with DAPI. Images were taken using a Zeiss automated inverted epifluorescent microscope (×10, NA = 0.3) and a Zeiss LSM 710 inverted confocal microscope (×20, NA = 0.8). Zeiss's Zen software was used to acquire and process the images. A mouse anti-TH antibody (1:1,000; product ID: 22941, Immunostar) followed by labeling with an Alexa Fluor 488-conjugated goat anti-mouse (AB150113, Abcam) was used for imaging TH expression.

Statistics and reproducibility. GraphPad Prism 8 was used for statistical analysis and generation of graphs. SPSS was used for a three-way ANOVA comparison for assessing baseline differences in ARC^{AgRP} activity between SD and HFD groups across recording weeks between the fed and fasted states. For discrete comparisons between two groups, two-tailed *t*-tests were used. For comparisons across groups or between groups over time, repeated-measures one-way or two-way ANOVAs were used, respectively, with corresponding post hoc tests adjusted for multiple comparisons. Normality and equal variances were assumed. Mice were randomly assigned to groups but were matched for age, sex and body weights. Experimenters were not blinded to conditions during testing and analysis owing to the necessity to only test HFD-exposed mice with HFD access, as well as the visibly clear differences in body weights after chronic HFD. Power analyses were not used to determine sample sizes; however, group sizes were chosen to match similar studies[9–11].

Reporting Summary. Further information on research design is available in the Nature Research Reporting Summary linked to this article.

Data availability

Data and supporting materials will be made available by the corresponding authors upon reasonable request.

Code availability

Code is available by the corresponding authors upon request or directly at https://www.niehs.nih.gov/research/atniehs/labs/ln/pi/iv/tools/index.cfm.

References

50. Madisen, L. et al. A robust and high-throughput Cre reporting and characterization system for the whole mouse brain. *Nat. Neurosci.* **13**, 133–140 (2010).
51. Meng, C. et al. Spectrally resolved fiber photometry for multi-component analysis of brain circuits. *Neuron* **98**, 707–717 (2018).
52. Nguyen, K. P., O'Neal, T. J., Bolonduro, O. A., White, E. & Kravitz, A. V. Feeding Experimentation Device (FED): a flexible open-source device for measuring feeding behavior. *J. Neurosci. Methods* **267**, 108–114 (2016).

Acknowledgements

Research was supported by an NIEHS–NIDDK joint fellowship. We thank N. Martin and B. Gloss of the NIEHS Viral Vector Core for producing AAVs and J. Tucker of the NIEHS Fluorescence Microscopy and Imaging Center for assistance with image acquisition. We thank the GENIE project for the development of GCaMP6. We would also like to thank all members of Dr. Krashes' and Dr. Cui's labs for their technical support and guidance throughout this work and J. Cushman of the NIEHS Neurobehavioral Core for assistance with behavioral studies and statistical analyses. This work was supported by the Intramural Research Program of the National Institutes of Health, the National Institute of Environmental Health Sciences (1ZIAES103310 to G.C.), the National Institutes of Diabetes and Digestive and Kidney Diseases (DK075088 to M.J.K. and DK075087-06 to M.J.K.), the NIEHS–NIDDK Joint Fellowship Award (to C.M.M.) and the Center of Compulsive Behaviors (to C.M.M. and I.D.A.S.).

Author contributions

C.M.M., J. L.-G. and M.J.K. designed experiments with technical input from G.C., J. L.-G., N.S.W. and M.H.B. M.S. performed and analyzed home cage consumption and body composition, fast–refeed and optogenetic experiments. C.M.M. performed and analyzed home cage AgRP fiber photometry experiments and DA sensor experiments. C.L. performed and analyzed LepR-Cre fiber photometry experiments. C.L. and I.D.A.S. performed electrophysiology recordings. J. L.-G. performed and analyzed gastric infusion and VTA studies. F.S., Y.Z. and Y.L. provided the DA2m sensor and provided technical guidance. N.P.K. and D.M.R. performed histological verification and imaging. C.M.M., J. L.-G. and M.J.K. wrote the manuscript with input from G.C., C.L., I.D.A.S., N.S.W., M.H.B., M.S., N.P.K., D.M.R., F.S, Y.Z. and Y.L.

Competing interests

The authors declare no competing interests.

Additional information

Extended data is available for this paper at https://doi.org/10.1038/s41593-020-0684-9.

Supplementary information is available for this paper at https://doi.org/10.1038/s41593-020-0684-9.

Correspondence and requests for materials should be addressed to G.C. or M.J.K.

Peer review information *Nature Neuroscience* thanks Paul Kenny and the other, anonymous, reviewer(s) for their contribution to the peer review of this work.

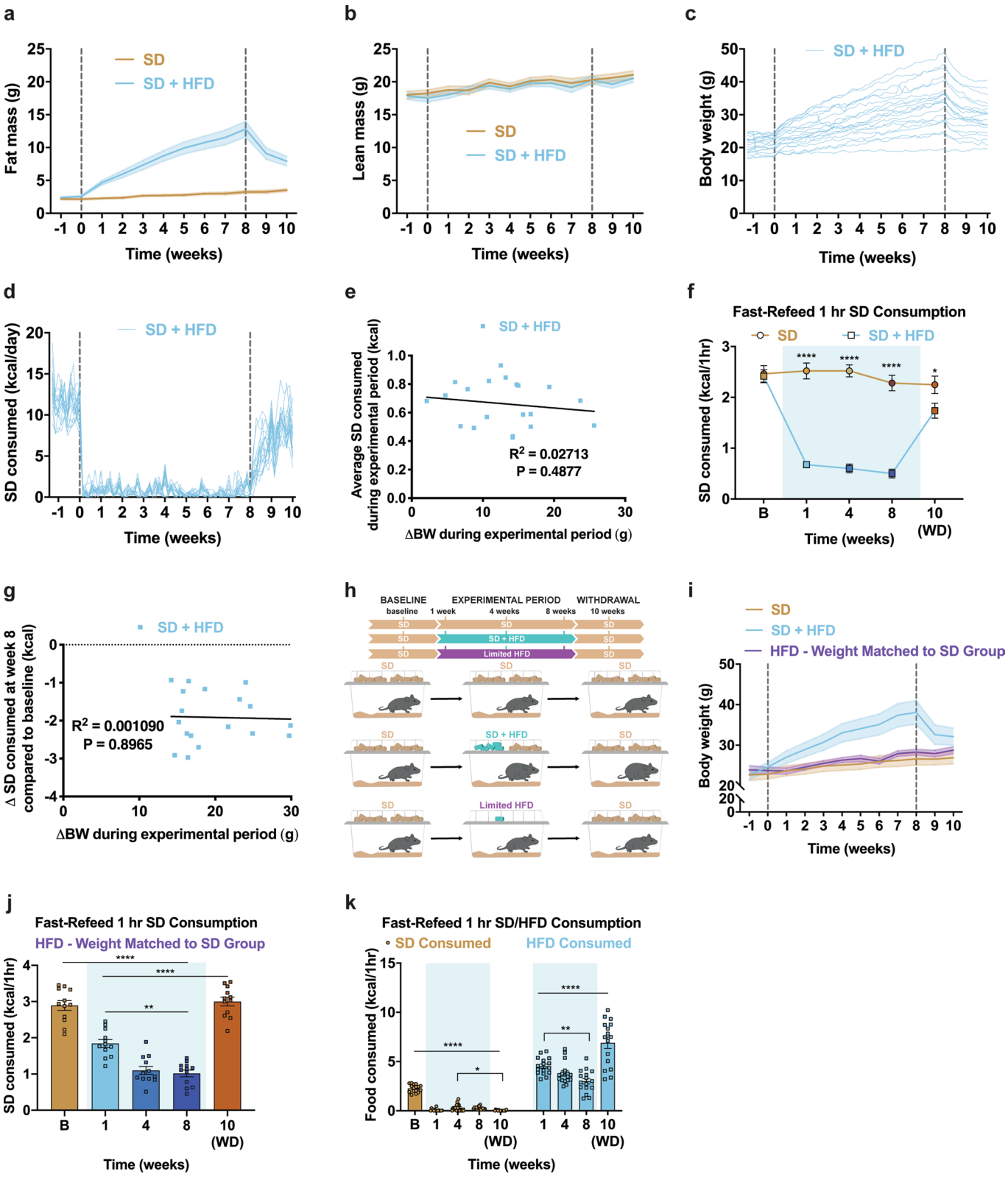

Extended Data Fig. 1 | See next page for caption.

Extended Data Fig. 1 | HFD-exposure promotes fat mass accrual, reduction of homecage SD intake and devaluation of SD in physiologically hungry mice independent of weight gain. Weekly **a**, fat mass (n = 20, males and females, RM two-way ANOVA, Week x Group: $F(11, 418) = 50.17$, $P < 0.0001$, Sidak's multiple comparisons test) and **b**, lean mass throughout diet exposure (n = 20, males and females, RM two-way ANOVA, Week x Group: $F(11, 418) = 0.8075$, $P = 0.6326$). Daily **c**, body weights and **d**, SD intake throughout the duration of the experiment of individual animals exposed to HFD. **e**, No correlation between the average amount of SD intake during the HFD-exposure period and body weight changes after 8 weeks of SD and HFD access (n = 20, males and females, Linear regression, $R^2 = 0.02713$, $P = 0.4877$). **f**, Between-subject comparison of 1 hr SD fast-refeed consumption across test sessions (n = 16 SD group, n = 18 SD + HFD group, males and females, RM two-way ANOVA, Time x Group: $F(4, 128) = 28.99$, $P < 0.0001$, Bonferroni's multiple comparisons test). **g**, No correlation between SD devaluation at Week 8 relative to Baseline and body weight changes after 8 weeks of access to SD and HFD (n = 18, males and females, Linear regression, $R^2 = 0.001090$, $P = 0.8965$). **h**, Experimental timeline, group schematic for home cage measurements and **i**, and daily body weights throughout the duration of the experiment (n = 12 per group, males and females). **j**, Within-subject comparison of 1 hr SD fast-refeed consumption across testing sessions (n = 12 limited HFD weight-matched to SD group, males and females, RM one-way ANOVA, Time: $F(2.431, 26.74) = 66.81$, $P < 0.0001$, Tukey's multiple comparisons). **k**, Within-subject, within-diet comparisons of 1 hr SD and HFD fast-refeed consumption across testing sessions (n = 18, males and females, RM one-way ANOVAs, Tukey's multiple comparisons). Dotted lines in **a–d** and **i** delineate window of HFD availability. All error bars and shaded areas in **a, b** and **i** represent mean ± s.e.m. Shaded blue area in **f**, **j**, and **k** represent HFD homecage availability. $^{*}P < 0.05$, $^{**}P < 0.01$, $^{****}P < 0.0001$.

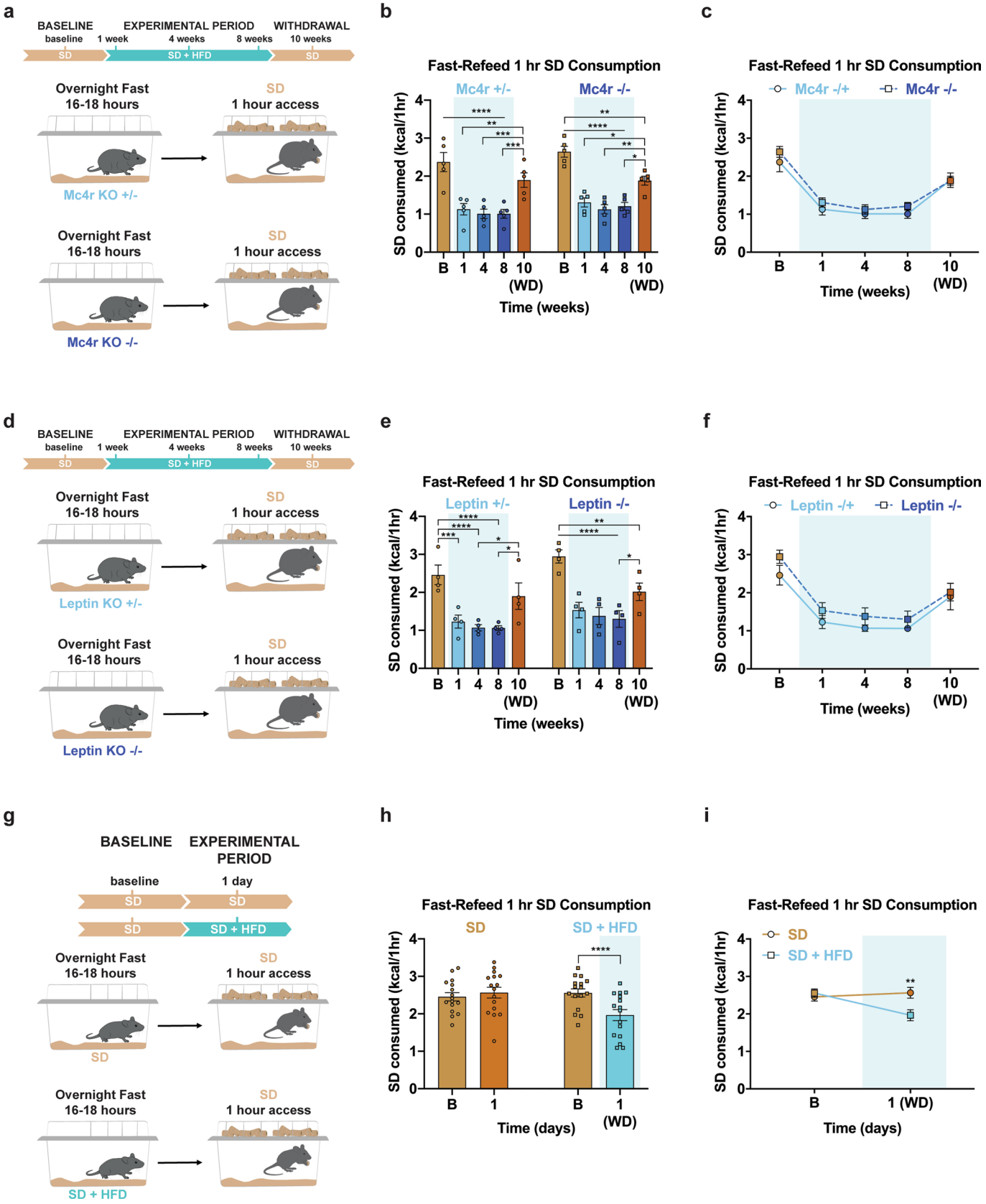

Extended Data Fig. 2 | See next page for caption.

Extended Data Fig. 2 | Intact melanocortin-4 receptor- or leptin-signaling are dispensable for SD devaluation following HFD-exposure and 24 h of HFD-exposure is sufficient to devalue SD. a, d Experimental timeline and group schematic for fast-refeed test with 1 hr SD access. **b, e** Within-subject and **c, f** between-subject comparisons of 1 hr SD fast-refeed consumption across testing sessions (n = 5 per Mc4r KO +/- and -/- group, males and females, RM two-way ANOVA, Time x Group: F (4, 32) = 0.3173, P = 0.8643, Tukey's multiple comparisons) (n = 4 per Leptin KO +/- and -/- group, males and females, RM two-way ANOVA, Time x Group: F (4, 24) = 0.3313, P = 0.8542, Tukey's multiple comparisons). **g**, Experimental timeline and group schematic for fast-refeed test with 1 hr SD access. **h**, Within-subject and **i**, between-subject comparisons of 1 hr SD fast-refeed consumption across testing sessions (n = 16 per group, males and females, RM two-way ANOVA, Time x Group: F (1, 30) = 16.96, P = 0.0003, Sidak's multiple comparisons test). B = Baseline. WD = withdrawal. Shaded blue area in **b**, **c**, **e**, **f**, **h** and **i** represent HFD homecage availability. All error bars represent s.e.m. $^{*}P < 0.05$, $^{**}P < 0.01$, $^{***}P < 0.001$, $^{****}P < 0.0001$.

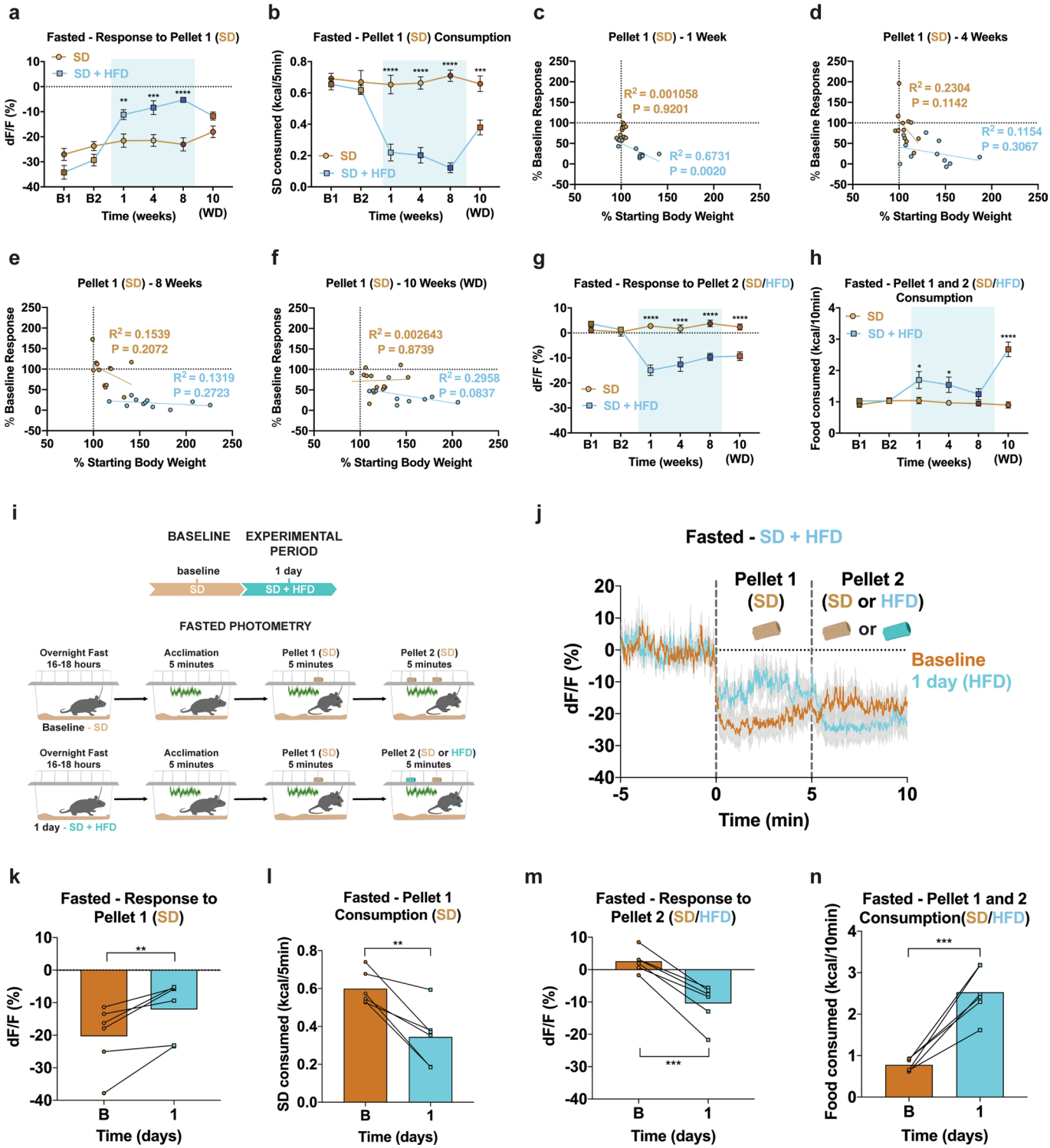

Extended Data Fig. 3 | See next page for caption.

Extended Data Fig. 3 | Acute and chronic HFD-exposure alters ARC^{AgRP} activity responses to SD and HFD in fasted mice largely independent of body-weight changes. a, Between-subject quantification of fasted ARC^{AgRP} activity response to Pellet 1 (SD) (n = 12 SD group, n = 11 SD + HFD group, males and females, RM two-way ANOVA, Time x Group: $F(5, 105) = 16.74$, $P < 0.0001$, Bonferroni's multiple comparisons) and **b**, SD consumed across testing sessions (n = 12 SD group, n = 11 SD + HFD group, males and females, RM two-way ANOVA, Time x Group: $F(5, 105) = 15.81$, $P < 0.0001$, Bonferroni's multiple comparisons). **c–f**, ARC^{AgRP} activity changes to Pellet 1 (SD) presentation are not strongly correlated with bodyweight accrual over the entire length of the experiment (n = 12 SD group, n = 11 SD + HFD group, males and females, Linear regression, **c**, SD group: $R^2 = 0.001058$, $P = 0.9201$, SD + HFD group: $R^2 = 0.6731$, $P = 0.0020$, **d**, SD group: $R^2 = 0.2304$, $P = 0.1142$, SD + HFD group: $R^2 = 0.1154$, $P = 0.3067$, **e**, SD group: $R^2 = 0.1539$, $P = 0.2072$, SD + HFD group: $R^2 = 0.1319$, $P = 0.2723$, **f**, SD group: $R^2 = 0.002643$, $P = 0.8739$, SD + HFD group: $R^2 = 0.2958$, $P = 0.0837$) **g**, Between-subject quantification of fasted ARC^{AgRP} activity response to Pellet 2 (SD for SD group; SD for SD + HFD group during B1 and B2 and HFD for SD + HFD group during 1, 4, 8 and 10 weeks) (n = 12 SD group, n = 11 SD + HFD group, males and females, RM two-way ANOVA, Time x Group: $F(5, 105) = 21.07$, $P < 0.0001$, Bonferroni's multiple comparisons) and **h**, total calories consumed across testing sessions (n = 12 SD group, n = 11 SD + HFD group, males and females, RM two-way ANOVA, Time x Group: $F(5, 105) = 14.26$, $P < 0.0001$, Bonferroni's multiple comparisons). **i**, Experimental timeline and group schematic for fasted photometry recordings. **j**, Average fasted photometry traces across recording sessions aligned to Pellet 1 and 2 presentation (n = 6, males and females). **k**, Within-subject quantification of fasted ARC^{AgRP} activity response to Pellet 1 (SD) (n = 6, males and females, Paired t test (two-tailed), $P = 0.0099$) and **l**, SD consumed across testing sessions (n = 6, males and females, Paired t test (two-tailed), $P = 0.0049$). **m**, Within-subject quantification of fasted ARC^{AgRP} activity response to Pellet 2 (SD for Baseline; HFD for 1 day) (n = 6, males and females, Paired t test (two-tailed), $P = 0.0008$) and **n**, total calories consumed across testing sessions (n = 6, males and females, Paired t test (two-tailed), $P = 0.0008$). Shaded blue area in **a, b**, and **g, h** represent HFD homecage availability. B1 and B2 refer to Baseline 1 and 2, respectively. WD = withdrawal. Dotted lines in **j** indicate Pellet 1 and Pellet 2 presentation. All error bars and shaded regions of **j** represent s.e.m. $^{*}P < 0.05$, $^{**}P < 0.01$, $^{***}P < 0.001$, $^{****}P < 0.0001$.

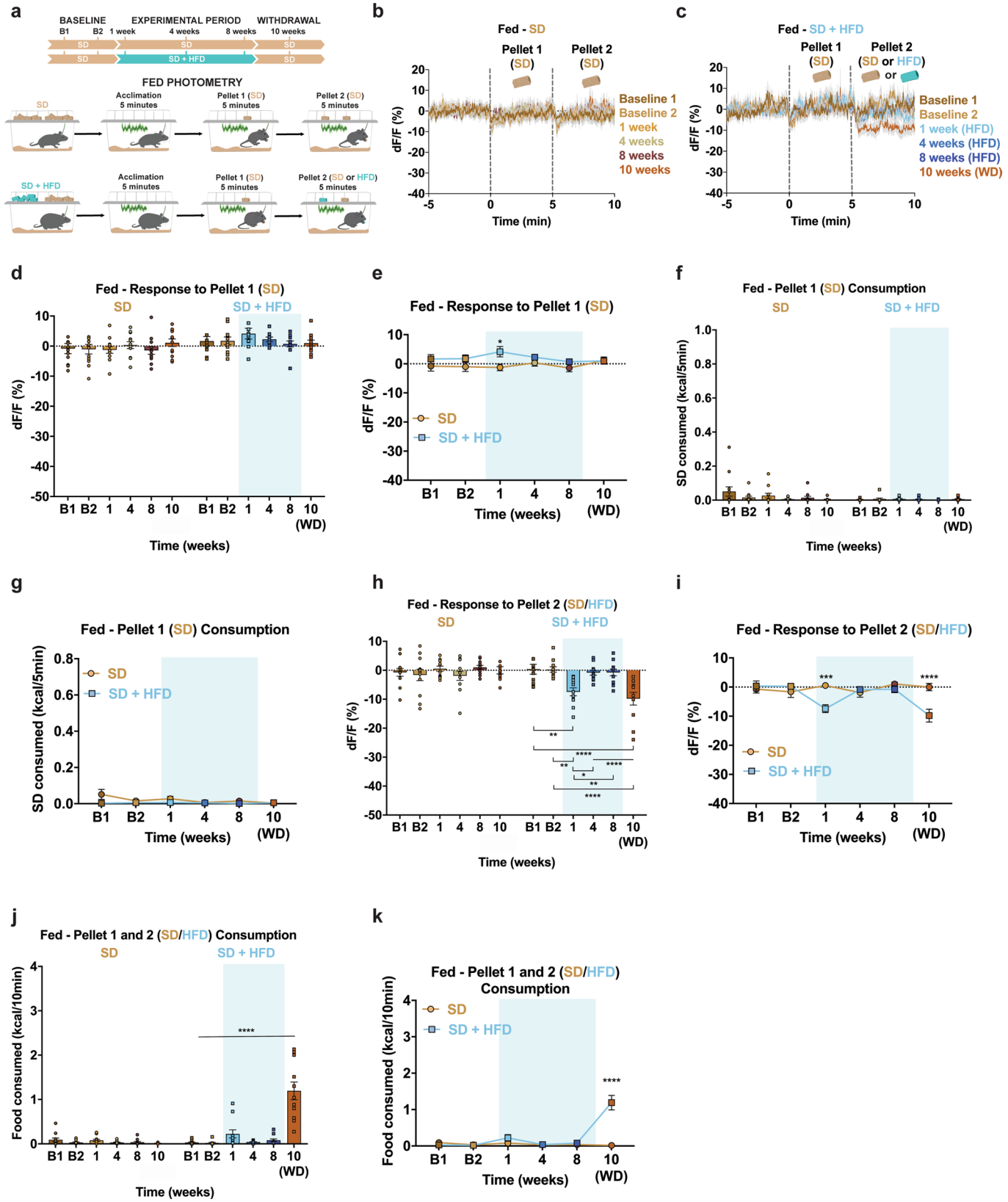

Extended Data Fig. 4 | See next page for caption.

Extended Data Fig. 4 | HFD-exposure alters ARC^{AgRP} activity responses to HFD in fed mice. a, Experimental timeline and group schematic for fed photometry recordings. **b, c**, Average fed photometry traces of the **b**, SD group and **c**, SD + HFD group across recording sessions aligned to Pellet 1 and 2 presentation (n = 12 SD group, n = 11 SD + HFD group, males and females). **d**, Within- and **e**, between-subject quantification of fed ARC^{AgRP} activity response to Pellet 1 (SD) (n = 12 SD group, n = 11 SD + HFD group, males and females, RM two-way ANOVA, Time x Group: $F(5, 105) = 0.8953$, $P = 0.4872$, Bonferroni's multiple comparisons). **f**, Within- and **g**, between-subject quantification of SD consumed across testing sessions (n = 12 SD group, n = 11 SD + HFD group, males and females, RM two-way ANOVA, Time x Group: $F(5, 105) = 1.768$, $P = 0.1258$). **h**, Within- and **i**, between-subject quantification of fed ARC^{AgRP} activity response to Pellet 2 (SD for SD group; SD for SD + HFD group during B1 and B2 and HFD for SD + HFD group during 1, 4, 8 and 10 weeks) (n = 12 SD group, n = 11 SD + HFD group, males and females, RM two-way ANOVA, Time x Group: $F(5, 105) = 7.565$, $P < 0.0001$, Bonferroni's multiple comparisons). **j**, Within- and **k**, between-subject quantification of total calories consumed across testing sessions (n = 12 SD group, n = 11 SD + HFD group, males and females, RM two-way ANOVA, Time x Group: $F(5, 105) = 31.68$, $P < 0.0001$, Bonferroni's multiple comparisons). Dotted lines in **b, c** indicate Pellet 1 and Pellet 2 presentation. Shaded blue area in **d–k** represent HFD homecage availability. B1 and B2 refer to Baseline 1 and 2, respectively. WD = withdrawal. All error bars and shaded regions of **b, c** represent s.e.m. $^{*}P < 0.05$, $^{**}P < 0.01$, $^{***}P < 0.001$, $^{****}P < 0.0001$.

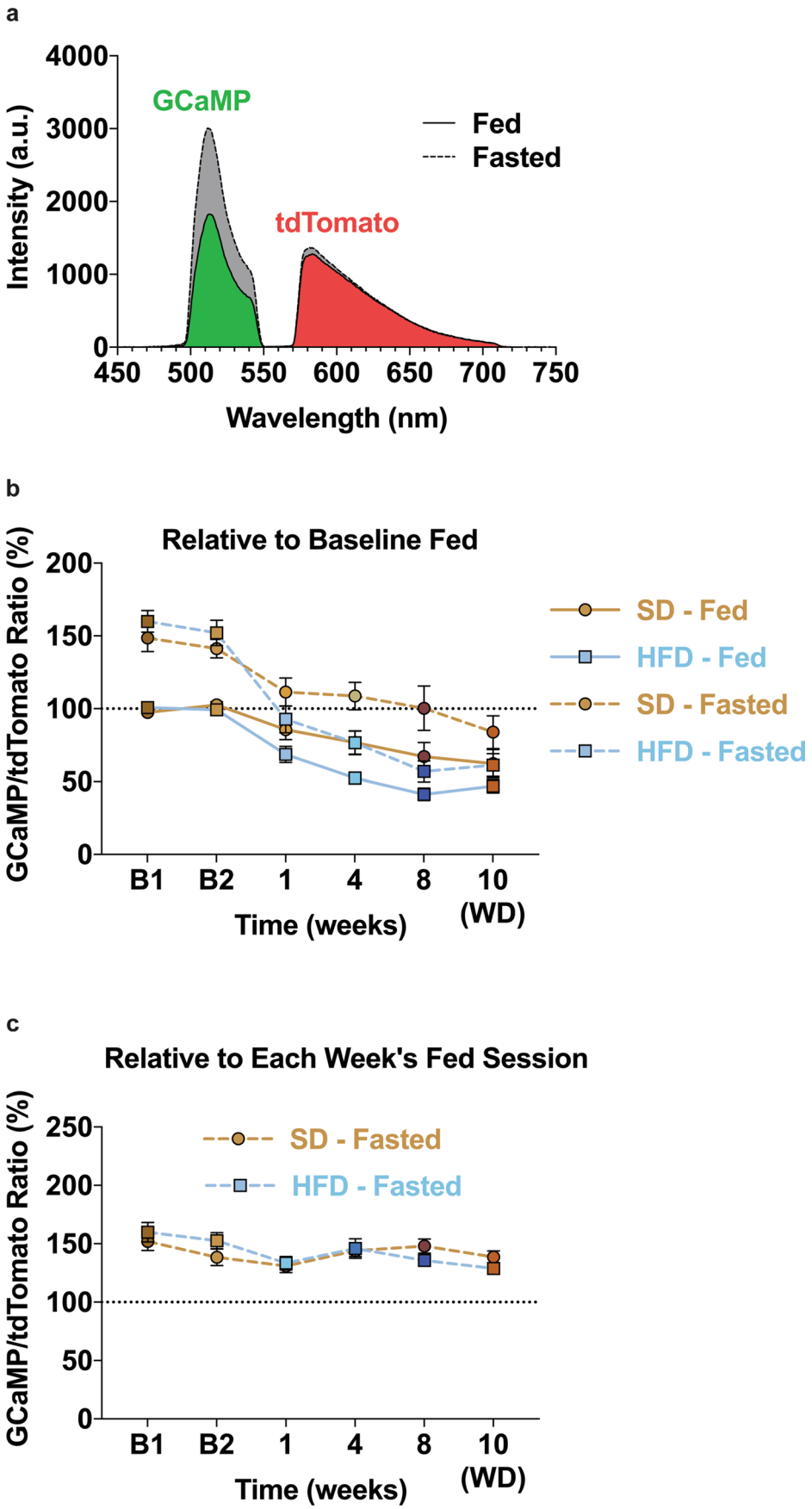

Extended Data Fig. 5 | See next page for caption.

Extended Data Fig. 5 | Spectrum-based fiber photometry reveals diminished ARC^{AgRP} baseline activity following HFD exposure. a, Representative GCaMP and tdTomato emission spectra from a mouse during the Fed and Fasted sessions of Baseline 1 prior to the addition of food. **b**, GCaMP/tdTomato ratios normalized to the mean of Baseline 1 + 2 Fed values shows basal ARC^{AgRP} activity is increased during Fasted sessions relative to Fed sessions (SD – Fed vs Fasted; HFD – Fed vs Fasted). Homecage HFD exposure reduces basal ARC^{AgRP} activity relative to the SD group across both Fed and Fasted conditions (Fed – SD vs HFD; Fasted – SD vs HFD) (n = 12 SD group, n = 11 SD + HFD group, males and females, three-way ANOVA, Diet: $F(1,21) = 6.515$, $P = 0.019$, Satiety state: $F(1,63) = 94.128$, $P < 0.0001$) **c**, Fasted GCaMP/tdTomato ratios normalized to the Fed values across recording sessions demonstrates an ~50% fasting-induced increase in the GCaMP/tdTomato ratio across all recording weeks (n = 12 SD group, n = 11 SD + HFD group, males and females, RM two-way ANOVA, Time x Group: $F(5, 105) = 1.978$, $P = 0.0879$). B1 and B2 refer to Baseline 1 and 2, respectively. WD = withdrawal.

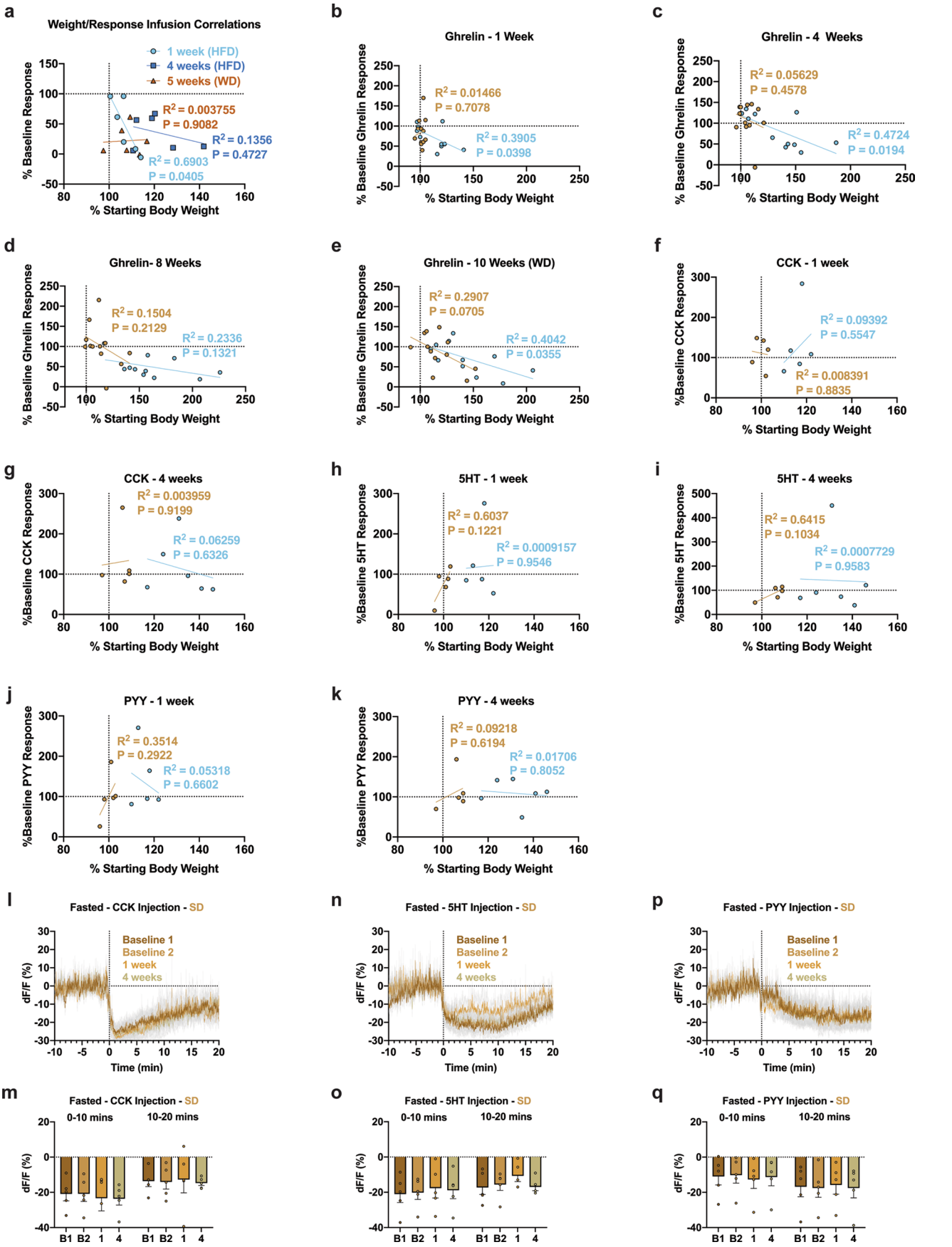

Extended Data Fig. 6 | See next page for caption.

Extended Data Fig. 6 | Physiological disruption of ARC^{AgRP} activity in response to HFD-exposure is partially dependent on body weight gain. a, Changes in ARC^{AgRP} activity in response to identical caloric load is correlated to weight gain 1, but not 4 weeks after HFD exposure or 1 week HFD withdrawal (n = 6, males and females, Linear regression, 1 week (HFD): $R^2 = 0.6903$, $P = 0.0405$, 4 weeks (HFD): $R^2 = 0.1356$, $P = 0.4727$, 5 weeks (WD): $R^2 = 0.003755$, $P = 0.9082$). **b-e**, Changes in ARC^{AgRP} activity in response to ghrelin is correlated to weight gain (n = 12 SD group, n = 11 SD + HFD group, males and females, Linear regression, **b**, SD group: $R^2 = 0.01466$, $P = 0.7078$, SD + HFD group: $R^2 = 0.3905$, $P = 0.0398$, **c**, SD group: $R^2 = 0.05629$, $P = 0.4578$, SD + HFD group: $R^2 = 0.4724$, $P = 0.0194$, **d**, SD group: SD group: $R^2 = 0.1504$, $P = 0.2129$, SD + HFD group: $R^2 = 0.2336$, $P = 0.1321$), **e**, SD group: $R^2 = 0.2907$, $P = 0.0705$, SD + HFD group: $R^2 = 0.4042$, $P = 0.0355$. **f-k**, Changes in ARC^{AgRP} activity in response to **f, g**, CCK, **h–l**, 5HT or **j, k**, PYY is not correlated to weight gain (n = 5 SD group, n = 6 SD + HFD group, males and females, Linear regression, **f**, SD group: $R^2 = 0.008391$, $P = 0.8835$, SD + HFD group: $R^2 = 0.09392$, $P = 0.5547$, **g**, SD group: $R^2 = 0.003959$, $P = 0.9199$, SD + HFD group: $R^2 = 0.06259$, $P = 0.6326$, **h**, SD group: $R^2 = 0.6037$, $P = 0.1221$, SD + HFD group: $R^2 = 0.0009157$, $P = 0.9546$, **i**, SD group: $R^2 = 0.6415$, $P = 0.1034$, SD + HFD group: $R^2 = 0.0007729$, $P = 0.9583$, **j**, SD group: $R^2 = 0.3514$, $P = 0.2922$, SD + HFD group: $R^2 = 0.05138$, $P = 0.6602$, **k**, SD group: $R^2 = 0.09218$, $P = 0.6194$, SD + HFD group: $R^2 = 0.01706$, $P = 0.8052$). **l, n, p**, Average photometry traces of the SD group across recording sessions aligned to **l**, CCK, **n**, 5HT or **p**, PYY injection (n = 5 SD group, males and females). **m, o, q**, Within-subject quantification of ARC^{AgRP} activity to **m**, CCK (n = 5 SD group, males and females, RM two-way ANOVA, Time Bin x Week: $F(1.511, 6.045) = 1.014$, $P = 0.3923$), **o**, 5HT (n = 5 SD group, males and females, RM two-way ANOVA, Time Bin x Week: $F(2.334, 9.337) = 1.242$, $P = 0.3393$) or **q**, PYY (n = 5 SD group, males and females, RM two-way ANOVA, Time Bin x Week: $F(1.897, 7.589) = 1.885$, $P = 0.2164$) across testing sessions. Dotted lines indicate **l**, CCK, **n**, 5HT or **p**, PYY injection. B1 and B2 refer to Baseline 1 and 2, respectively. All error bars and shaded regions of **l, n**, and **p** represent s.e.m.

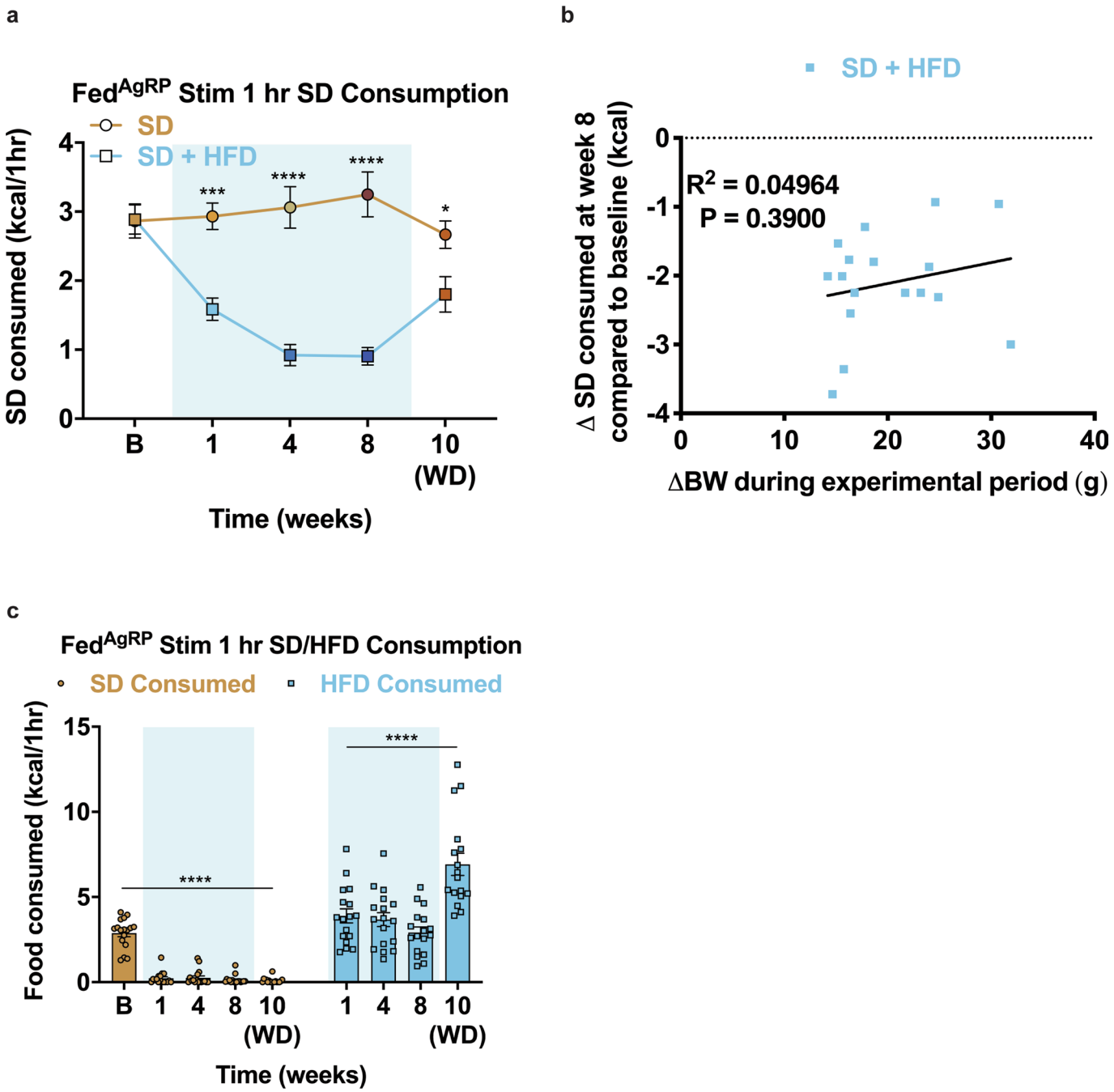

Extended Data Fig. 7 | HFD exposure promotes devaluation of optogenetic ARC^{AgRP}-evoked SD, but not HFD, and consumption independent of weight gain. a, Between-subject comparison of fed^{AgRP} stimulation 1 hr SD consumption across test sessions (n = 16 SD group, n = 17 SD + HFD group, males and females, RM two-way ANOVA, Time x Group: $F(4, 124) = 18.85$, $P < 0.0001$, Bonferroni's multiple comparisons). **b**, No correlation between SD devaluation at Week 8 relative to Baseline and body weight changes after 8 weeks of access to SD and HFD (n = 17, males and females, Linear regression, $R^2 = 0.04964$, $P = 0.3900$). **c**, Within-subject, within-diet comparisons of fed^{AgRP} stimulation 1 hr SD and HFD consumption across testing sessions (n = 17, males and females, RM one-way ANOVAs, Tukey's multiple comparisons). B = Baseline. WD = Withdrawal. Shaded blue area in **a** and **c** represent HFD homecage availability. All error bars represent s.e.m. $^{*}P < 0.05$, $^{**}P < 0.01$, $^{***}P < 0.001$, $^{****}P < 0.0001$.

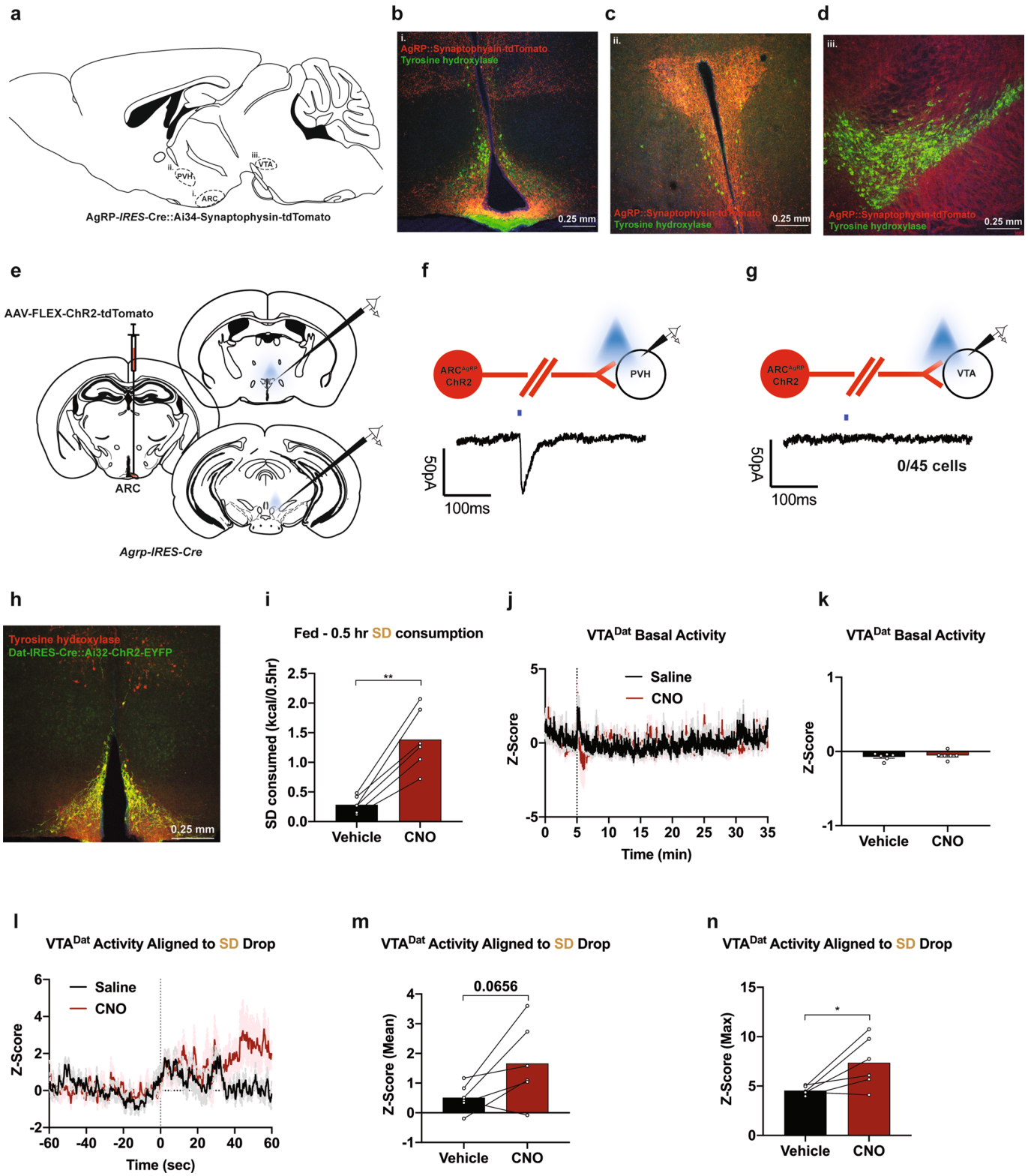

Extended Data Fig. 8 | ARC$^{AgRP/Npy}$ activation does not alter basal VTA^{Dat} activity but potentiates signaling in response to food via an indirect signaling mechanism. a, Brain schematic of anterograde tracing strategy. **b–d**, representative images of AgRP::Synaptophysin-tdTomato and tyrosine hydroxylase (TH) in the **b**, arcuate nucleus, **c**, paraventricular hypothalamus and **d**, ventral tegmental area. **e**, Brain schematic of unilateral viral delivery of Cre-inducible ChR2 to the ARC of AgRP-ires-Cre mice and position of ex vivo slice recordings from PVH (top) and VTA (bottom) cells. **f, g**, ChR2-assisted circuit mapping schematic and representative trace from **f**, PVH and **g**, VTA cells. **h**, Representative image of Dat-ires-Cre::Ai32-ChR2-eYFP and overlap with TH in the ARC. **i**, Chemogenetic ARC^{Npy} activation drives food intake (n = 6, males and females, Paired t test (two-tailed), P = 0.0013). **j**, Averaged Z-score traces and **k**, quantification of basal VTA^{Dat} activity after saline or CNO injections (n = 6, males and females, Paired t test (two-tailed), P = 0.2837). **l**, Averaged Z-score traces and **m**, mean (n = 6, males and females, Paired t test (two-tailed), P = 0.0656) and **n**, max quantification (n = 6, males and females, Paired t test (two-tailed), P = 0.0365) of VTA^{Dat} activity in response to SD food drop after saline or CNO injections. All error bars represent s.e.m. $^{*}P < 0.05$, $^{**}P < 0.01$.

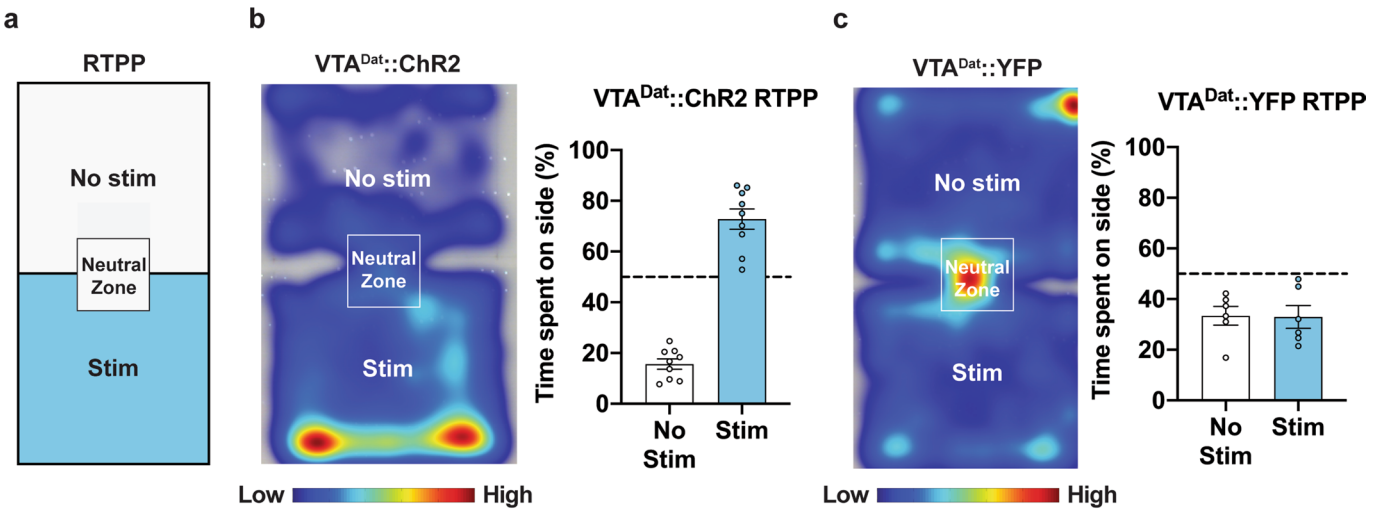

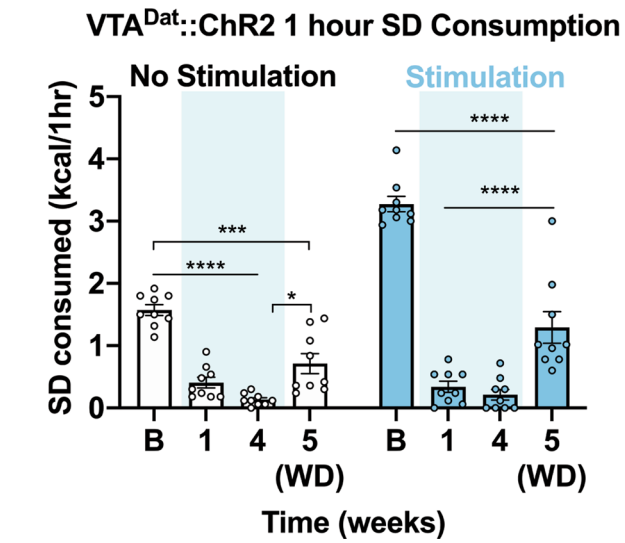

Extended Data Fig. 9 | VTA^{Dat} photostimulation is intrinsically rewarding but loses the capacity to enhance SD consumption in fasted mice after HFD exposure. a, Schematic of Real-Time Place Preference assay. **b**, Averaged heat maps and quantification of time spent in each chamber of the RTPP assay in VTA^{Dat}::ChR2 mice (n = 9, males, Paired t test (two-tailed), $P < 0.0001$). c, Averaged heat maps and quantification of time spent in each chamber of the RTPP assay in control VTA^{Dat}::YFP mice (n = 6, males, Paired t test (two-tailed), $P = 0.9576$). **d**, Within-subject and condition comparisons of 1 hr SD consumption across testing sessions with or without VTA^{Dat} photostimulation (n = 9, males, RM two-way ANOVA, Time x Condition: $F(3, 48) = 18.30$, $P < 0.0001$, Tukey's multiple comparisons). B = Baseline. WD = Withdrawal. Shaded blue area in **d** represents HFD homecage availability. All error bars represent s.e.m. $^{***}P < 0.001$, $^{****}P < 0.0001$.

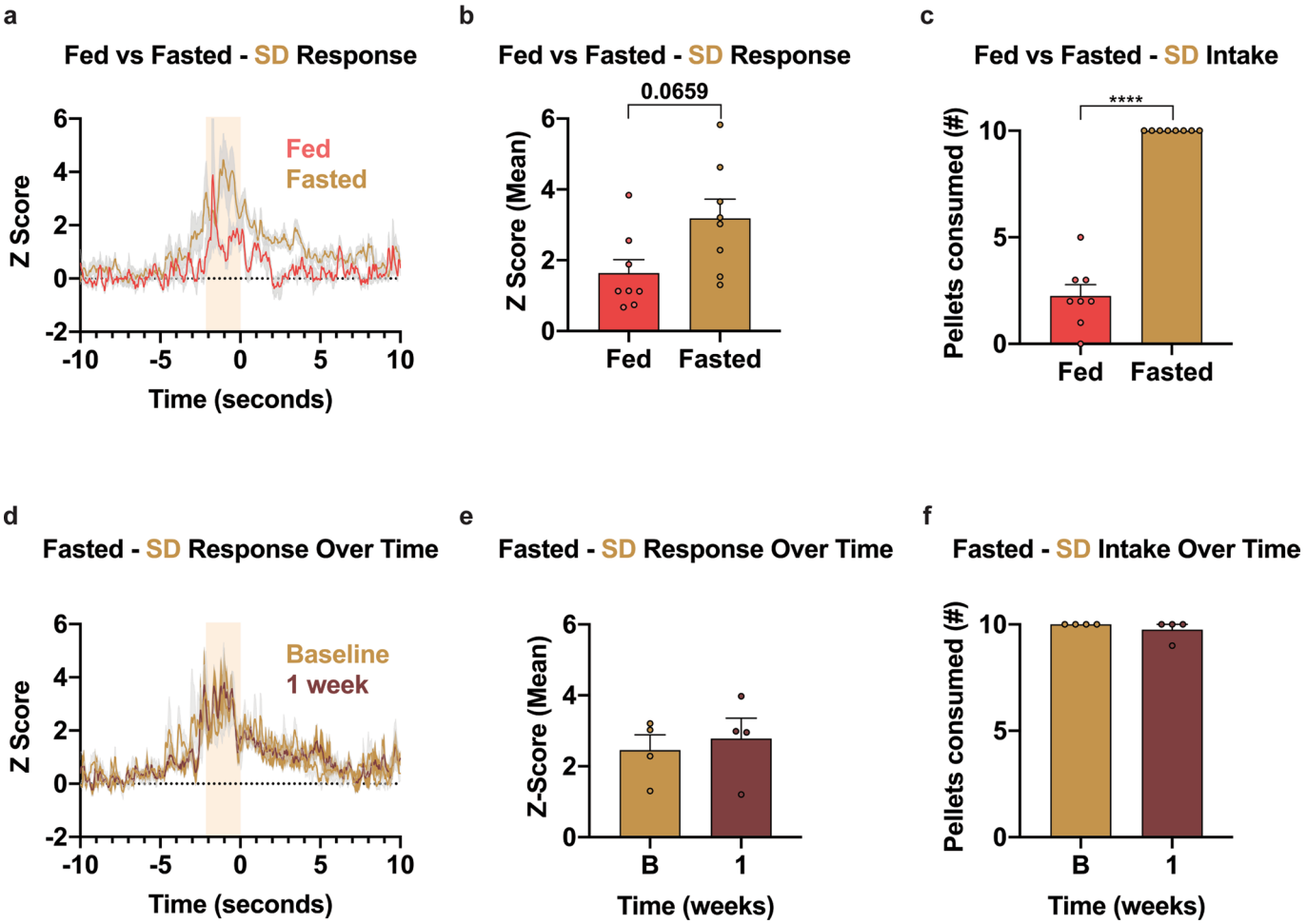

Extended Data Fig. 10 | DA responses to SD are state-dependent and consistent over time in HFD-naïve animals. a, Averaged Z-score traces of DA2m fluorescence aligned to SD pellet retrieval across appetite state (n = 8, males and females). **b**, Within-subject comparisons of mean fluorescence Z-score during SD pellet retrieval across appetite state (n = 8, males and females, Paired t test (two-tailed), P = 0.0659). **c**, Within-subject comparisons of SD pellets consumed across appetite state (n = 8, males and females, Paired t test (two-tailed), P < 0.0001). **d**, Averaged Z-score traces of DA2m fluorescence aligned to SD pellet retrieval across recording weeks. (n = 4, males and females) **e**, Within-subject comparisons of mean fluorescence Z-score during SD pellet retrieval across sessions (n = 4, males and females, Wilcoxon matched-pairs signed rank test, P = 0.625). **f**, Within-subject comparisons of SD pellets consumed across sessions (n = 4, males and females, Wilcoxon matched-pairs signed rank test, P > 0.9999). Time 0 denotes consumption. B = Baseline. Shaded peach region in **a** and **d** represent quantified pellet approach/retrieval period. All error bars and shaded regions of **a** and **d** represent s.e.m. ****$P < 0.0001$.

nature research

Corresponding author(s): Michael J. Krashes

Last updated by author(s): 06/24/2020

Reporting Summary

Nature Research wishes to improve the reproducibility of the work that we publish. This form provides structure for consistency and transparency in reporting. For further information on Nature Research policies, see Authors & Referees and the Editorial Policy Checklist.

Statistics

For all statistical analyses, confirm that the following items are present in the figure legend, table legend, main text, or Methods section.

n/a	Confirmed	
☐	☒	The exact sample size (*n*) for each experimental group/condition, given as a discrete number and unit of measurement
☐	☒	A statement on whether measurements were taken from distinct samples or whether the same sample was measured repeatedly
☐	☒	The statistical test(s) used AND whether they are one- or two-sided *Only common tests should be described solely by name; describe more complex techniques in the Methods section.*
☐	☒	A description of all covariates tested
☐	☒	A description of any assumptions or corrections, such as tests of normality and adjustment for multiple comparisons
☐	☒	A full description of the statistical parameters including central tendency (e.g. means) or other basic estimates (e.g. regression coefficient) AND variation (e.g. standard deviation) or associated estimates of uncertainty (e.g. confidence intervals)
☐	☒	For null hypothesis testing, the test statistic (e.g. *F*, *t*, *r*) with confidence intervals, effect sizes, degrees of freedom and *P* value noted *Give P values as exact values whenever suitable.*
☒	☐	For Bayesian analysis, information on the choice of priors and Markov chain Monte Carlo settings
☒	☐	For hierarchical and complex designs, identification of the appropriate level for tests and full reporting of outcomes
☒	☐	Estimates of effect sizes (e.g. Cohen's *d*, Pearson's *r*), indicating how they were calculated

Our web collection on statistics for biologists contains articles on many of the points above.

Software and code

Policy information about availability of computer code

Data collection	Tucker Davis Technologies Synapse, Oceanview, unmixing algorithm written in R, PatchClamp
Data analysis	GraphPad Prism 8.0, SPSS

For manuscripts utilizing custom algorithms or software that are central to the research but not yet described in published literature, software must be made available to editors/reviewers. We strongly encourage code deposition in a community repository (e.g. GitHub). See the Nature Research guidelines for submitting code & software for further information.

Data

Policy information about availability of data

All manuscripts must include a data availability statement. This statement should provide the following information, where applicable:

- Accession codes, unique identifiers, or web links for publicly available datasets
- A list of figures that have associated raw data
- A description of any restrictions on data availability

All data generated or analyzed during this study are included in this published article (and supplementary information files). Raw datasets are available from the corresponding author upon request.

Field-specific reporting

Please select the one below that is the best fit for your research. If you are not sure, read the appropriate sections before making your selection.

☒ Life sciences ☐ Behavioural & social sciences ☐ Ecological, evolutionary & environmental sciences

Life sciences study design

All studies must disclose on these points even when the disclosure is negative.

Sample size	Sample sizes were determined based on experience and standards in the field. All experiments were powered to give reproducible results.
Data exclusions	No data was excluded. Only animals that met pre-screening standards were used for experiments. i.e. animals with misplaced optical fibers that yielded no calcium signal obviously were not used for the studies.
Replication	Data have been independently obtained across laboratories in independent cohorts of animals.
Randomization	Mice were randomly assigned to different treatment groups but matched for sex, age and body weight
Blinding	Experiments with animals were not blinded.

Reporting for specific materials, systems and methods

We require information from authors about some types of materials, experimental systems and methods used in many studies. Here, indicate whether each material, system or method listed is relevant to your study. If you are not sure if a list item applies to your research, read the appropriate section before selecting a response.

Materials & experimental systems

n/a	Involved in the study
☐	☒ Antibodies
☒	☐ Eukaryotic cell lines
☒	☐ Palaeontology
☐	☒ Animals and other organisms
☒	☐ Human research participants
☒	☐ Clinical data

Methods

n/a	Involved in the study
☒	☐ ChIP-seq
☒	☐ Flow cytometry
☒	☐ MRI-based neuroimaging

Antibodies

Antibodies used	chicken anti-GFP (ab13970, Abcam), rabbit anti-RFP (ab62341, Abcam), Alexa Fluor 488 conjugated goat anti-chicken (A11039, Invitrogen) and Alexa Fluor 568 conjugated goat anti-rabbit (A11011, Invitrogen), mouse-anti-tyrosine hydroxylase (Product ID : 22941, Immunostar, Alexa Fluor 488 conjugated goat anti-mouse (ab150113, Abcam)
Validation	https://www.abcam.com/gfp-antibody-ab13970.html. "Validated in WB, IHC, ICC/IF. Cited in 1298 publication(s). Independently reviewed in 83 review(s)." https://www.abcam.com/rfp-antibody-ab62341.html. "Suitable for: IHC-P, IHC-FrFl, IHC-Fr, WB, IP, ICC/IF." https://www.citeab.com/antibodies/677127-22941-tyrosine-hydroxylase-antibody?utm_campaign=Widget+All+Citations&utm_medium=Widget&utm_source=ImmunoStar&utm_term=ImmunoStar

Animals and other organisms

Policy information about studies involving animals; ARRIVE guidelines recommended for reporting animal research

Laboratory animals	See materials and methods section. All animals including Jax numbers are provided there in detail.
Wild animals	*Provide details on animals observed in or captured in the field; report species, sex and age where possible. Describe how animals were caught and transported and what happened to captive animals after the study (if killed, explain why and describe method; if released, say where and when) OR state that the study did not involve wild animals.*
Field-collected samples	*For laboratory work with field-collected samples, describe all relevant parameters such as housing, maintenance, temperature, photoperiod and end-of-experiment protocol OR state that the study did not involve samples collected from the field.*
Ethics oversight	All animal protocols and procedures were approved by the US National Institute of Environmental Health Sciences Animal Care and Use Committee or the National Institutes of Health Animal Care and Use Committee.

Note that full information on the approval of the study protocol must also be provided in the manuscript.